

# Hypothalamic SLC7A14 accounts for aging-reduced lipolysis in white adipose tissue of male mice

Received: 29 October 2023

Accepted: 21 August 2024

Published online: 11 September 2024

 Check for updates

Xiaoxue Jiang<sup>1,3</sup>, Kan liu<sup>2,3</sup>, Peixiang Luo<sup>2</sup>, Zi Li<sup>2</sup>, Fei Xiao<sup>1</sup>, Haizhou Jiang<sup>1</sup>, Shangming Wu<sup>2</sup>, Min Tang<sup>1</sup>, Feixiang Yuan<sup>1</sup>, Xiaoying Li<sup>1</sup>, Yousheng Shu<sup>1</sup>, Bo Peng<sup>1</sup>, Shanghai Chen<sup>1</sup>, Shihong Ni<sup>1</sup> & Feifan Guo<sup>1</sup>✉

The central nervous system has been implicated in the age-induced reduction in adipose tissue lipolysis. However, the underlying mechanisms remain unclear. Here, we show the expression of SLC7A14 is reduced in proopiomelanocortin (POMC) neurons of aged mice. Overexpression of SLC7A14 in POMC neurons alleviates the aging-reduced lipolysis, whereas SLC7A14 deletion mimics the age-induced lipolysis impairment. Metabolomics analysis reveals that POMC SLC7A14 increased taurochenodeoxycholic acid (TCDCA) content, which mediates the SLC7A14 knockout- or age-induced WAT lipolysis impairment. Furthermore, SLC7A14-increased TCDCA content is dependent on intestinal apical sodium-dependent bile acid transporter (ASBT), which is regulated by intestinal sympathetic afferent nerves. Finally, SLC7A14 regulates the intestinal sympathetic afferent nerves by inhibiting mTORC1 signaling through inhibiting TSC1 phosphorylation. Collectively, our study suggests the function for central SLC7A14 and an upstream mechanism for the mTORC1 signaling pathway. Moreover, our data provides insights into the brain–gut–adipose tissue crosstalk in age-induced lipolysis impairment.

Obesity is a multifactorial chronic disease that is closely related to age<sup>1–3</sup>. Increased fat accumulation in older people is accompanied by age-induced reduction in white adipose tissue (WAT) lipolysis<sup>4,5</sup>. Adipocyte lipolysis is the hydrolysis of intracellular triacylglycerol into glycerol and fatty acids under the action of lipase. Age-induced reduction in lipolysis is caused by multiple factors<sup>2,3,5–7</sup>. The peripheral microenvironment of WAT, such as inflammation, plays an important role in this process<sup>4,5,8</sup>. In addition, the central nervous system (CNS) contributes to lipolysis reduction with age<sup>3,9,10</sup>. The hypothalamus is a key brain region involved in age-dependent obesity<sup>3</sup>. The arcuate nucleus (ARC) of the hypothalamus mainly contains two types of neurons, namely, agouti-related peptide/neuropeptide Y (AGRP/NPY) neurons and proopiomelanocortin (POMC)

neurons<sup>11</sup>. Recent studies have shown that the neuronal activity of POMC can regulate WAT lipolysis<sup>12</sup>. It is well known that central regulation of WAT lipolysis is mediated by direct activation of the sympathetic nervous system (SNS) in WAT<sup>12–14</sup>. There are some factors such as norepinephrine (NE), released at the nerve terminal, binds to  $\beta$ -adrenergic receptors, and increases intracellular levels of cyclic adenosine monophosphate (cAMP), which drives the phosphorylation of protein kinase A (PKA)-dependent lipase to complete lipolysis<sup>15</sup>. There are other manners to regulate lipolysis, such as via affecting inflammatory factors in macrophage<sup>16</sup> or hormones<sup>17–20</sup>. Recent studies have identified some metabolites as regulators of lipolysis<sup>16,21</sup>; however, it is unclear whether metabolites can mediate the effects of the CNS on lipolysis.

<sup>1</sup>Zhongshan Hospital, State Key Laboratory of Medical Neurobiology, Institute for Translational Brain Research, MOE Frontiers Center for Brain Science, Fudan University, Shanghai 200032, China. <sup>2</sup>CAS Key Laboratory of Nutrition, Metabolism and Food Safety, Innovation Center for Intervention of Chronic Disease and Promotion of Health, Shanghai Institute of Nutrition and Health, University of Chinese Academy of Sciences, Chinese Academy of Sciences, Shanghai 200031, China. <sup>3</sup>These authors contributed equally: Xiaoxue Jiang, Kan liu. ✉e-mail: [ffguo@fudan.edu.cn](mailto:ffguo@fudan.edu.cn)

Several hypothalamic signaling are shown to be important for lipolysis control. For example, in hypothalamus of aged mice, hypothalamic I $\kappa$ B kinase- $\beta$  (IKK $\beta$ ) and nuclear factor- $\kappa$ B (NF- $\kappa$ B) signaling is activated<sup>22</sup>, while autophagy and sirtuin-1 (SIRT1) signaling is suppressed<sup>23</sup>. Elderly mice with splicing factor 1 (SFI) deficiency in the hypothalamic ventromedial nucleus showed a significant increase in the fat weight<sup>10</sup>. In addition, the hypothalamic mechanistic target of rapamycin (mTOR) kinase signaling pathway is strongly associated with age-dependent obesity<sup>9</sup>. mTOR is a master regulator of cell growth and metabolism<sup>3,24</sup> that forms two complexes with different structures and functions, namely, mTORC1 and mTORC2. Both mTORC1 and mTORC2 signaling pathway are shown to be related to age-dependent obesity<sup>9,25</sup>. For example, recent studies have shown that the activation of mTOR in hypothalamic POMC neurons of aged mice results in the silencing of POMC neurons due to the activity of the ATP-sensitive potassium (K<sub>ATP</sub>) channel<sup>3,9</sup>. Injection of the mTOR inhibitor rapamycin into the brain of aging mice causes weight loss. Loss of mTORC2 in POMC neuron increased fat mass of aged mice<sup>25</sup>. The tuberous sclerosis complex (TSC), a GTPase activating protein (GAP) consisting of the TSC1 and TSC2, is a negative regulator of mTORC1<sup>26</sup>. Knockout of TSC1 in POMC neurons of young mice leads to obesity and silencing of POMC neurons, whereas the absence of TSC1 in AGRP neurons does not affect neuronal excitability or body weight<sup>3,9</sup>. However, the role of mTOR signaling and the regulatory mechanism in age-induced reduction in lipolysis remain poorly understood.

Solute carrier family 7 member 14 (SLC7A14) is a lysosomal membrane protein<sup>27,28</sup>. It has been indicated in the regulation of retina function<sup>29</sup>, auditory neuropathy<sup>30</sup>, as well as insulin resistance<sup>28</sup>, demonstrated by using global or tissue specific knockout mice. SLC7A14 is expressed in different tissues, most abundantly in the CNS<sup>28</sup>, but its central role is unclear. Based on the fact that mTORC2 activity is regulated by SLC7A14<sup>28</sup> and its subcellular location is on lysosome<sup>28</sup>, where mTORC1 activity significantly affected<sup>31</sup>, it is possible SLC7A14 functions as upstream regulator for mTOR. Because the hypothalamic mTOR signaling pathway is strongly associated with age-dependent obesity<sup>9</sup>, we speculated that hypothalamic SLC7A14 may play an important role in the aging-related increase in the fat mass via mTOR pathway. The aim of the current study was to investigate this hypothesis and explore the underlying mechanisms.

In this work, we demonstrate an important role for SLC7A14/mTORC1 signaling in POMC neurons in regulating age-induced reduction in lipolysis. Our findings show that POMC SLC7A14/mTORC1 signaling regulates lipolysis through TCDCA, without relying on the SNS in WAT, which is a new way of central regulation of lipolysis and upstream regulation of bile acids. Furthermore, our findings reveal the underlying mechanisms of the regulation of mTORC1 by SLC7A14. These results expand the understanding of the regulation of age-induced lipolysis impairment by the brain–gut–adipose tissue axis, provide insights into upstream regulation of bile acids.

## Results

### SLC7A14 expression is decreased in hypothalamic POMC neurons of aged mice and overexpression of SLC7A14 in POMC neurons alleviates age-induced reduction in WAT lipolysis

SLC7A14 is highly expressed in the central nervous system<sup>28,29</sup>. To clarify the distribution of SLC7A14 expression in brain, we examined its expression in different brain regions, and found the expression of SLC7A14 in hippocampus (HPO) and hypothalamus (HY) is higher than expression in cortex (COR), amygdala (AMY) and cerebellum (CB) (Fig. S1a). To elucidate the role of SLC7A14 in CNS in the regulation of lipolysis of adipocytes during aging, we examined the expression of SLC7A14 in the HPO and HY of young and aged male mice, and found that SLC7A14 expression did not change in the hippocampus (Fig. S1b),

but significantly decreased in the hypothalamus of aged mice (Fig. 1a), especially in the hypothalamic ARC (Fig. 1b).

Based on these results, we speculated that the decreased expression of SLC7A14 might play a role in aging-related metabolic phenotypes. Therefore, we examined the effect of SLC7A14 knockdown by injecting SLC7A14<sup>flax/flax</sup> male mice with adeno-associated virus expressing Cre (+ AAV-Cre) or green fluorescent protein (GFP; – AAV-Cre) in the hypothalamic ARC. The knockdown of SLC7A14 in the ARC, which was confirmed by measuring SLC7A14 mRNA and protein levels, did not change the body weight, but significantly increased body fat mass (Figs. S1c–g). Consistently, the weights of subcutaneous WAT (sWAT) and epididymal WAT (eWAT), but not that of brown adipose tissue (BAT), were increased (Fig. S1h). Histological analysis of sWAT showed that knockdown SLC7A14 in the ARC significantly enlarged the adipocyte size (Figs. S1i, j), but had no effect on sWAT cell numbers as determined by DNA content analysis (Fig. S1k). Next, we examined different processes of lipid metabolism in sWAT and found that the levels of phosphorylated hormone sensitive lipase (HSL), the rate-limiting enzyme for triglyceride lipolysis were significantly decreased, while those of other proteins related to fat metabolism, such as fatty acid synthase (FAS), CD36 Molecule (CD36), and carnitine palmitoyltransferase 1 $\alpha$  (CPT1 $\alpha$ ) did not change in sWAT of ARC SLC7A14 knockdown mice compared with those of control mice (Fig. S1l). Glycerol release analysis of sWAT further confirmed that the knockdown of SLC7A14 in the ARC significantly impaired lipolysis (Fig. S1m). In addition, the knockdown of SLC7A14 in the ARC did not change the expression of uncoupling protein 1 (UCP1) and histological analysis of BAT, as well as the rectal temperature (Figs. S1n–q). Furthermore, the daily food intake did not change in ARC SLC7A14 knockdown mice compared with that in control mice (Fig. S1r). These results suggest that the knockdown of SLC7A14 in the ARC mimics age-induced reduction in WAT lipolysis.

The ARC of the hypothalamus mainly includes AgRP neurons and POMC neurons<sup>31</sup>. We explored the cell specific expression of SLC7A14 in the hypothalamus using single-cell RNA seq (GSE188646). We found that SLC7A14 was mainly expressed in neurons defined by co-expression with *Syt1* (Figs. S2a–c). Further analysis showed that SLC7A14 was widely expressed in the neurons of hypothalamus, including AgRP and POMC neurons (Figs. S2d–f). To further clarify which neuron mediates the role of SLC7A14 in the ARC, aged AgRP-Cre or POMC-Cre male mice were injected with Cre-dependent AAV expressing SLC7A14 (+AAV-SLC7A14) or mCherry fluorescent protein (– AAV-SLC7A14) in AgRP or POMC neurons. The overexpression of SLC7A14 in AgRP neurons did not reverse aging-attenuated lipolysis, as demonstrated by an increase in the fat mass and inhibition of WAT lipolysis in aged mice, which was inconsistent with the effect of SLC7A14 in the ARC (Fig. S3). Next, we investigated the role of POMC SLC7A14 in lipid metabolism. SLC7A14 expression was decreased in hypothalamic POMC neurons of aged mice (Fig. 1c), which was consistent with the changes in the ARC (Fig. 1b). The overexpression of SLC7A14 in POMC neurons (SPOE) in aged mice decreased the fat mass, but not the lean mass, and reduced the weight of tissues, including sWAT and eWAT (Fig. 1d–g). Consistently, the size of adipocytes was much smaller in SPOE mice, associated with increased levels of p-HSL and p-PKA substrates, higher glycerol release ability and higher cAMP levels in sWAT (Fig. 1h–m). The expression of UCP1, cAMP levels, histological analysis in BAT and the rectal temperature did not change in SPOE mice (Figs. S4a–e). Furthermore, the food intake, oxygen consumption, heat, RER and locomotor activity did not differ between SPOE and control mice (Figs. S4f–j). These results indicate that overexpression of SLC7A14 in POMC neurons alleviated age-induced obesity, mainly by improving the age-induced reduction in WAT lipolysis.

## The absence of SLC7A14 in POMC neurons weakens WAT lipolysis

Based on the above results, we speculated that knockout of SLC7A14 in POMC neurons might mimic the age-induced lipolysis impairment. To test this hypothesis, we generated mice with SLC7A14 knockout in

POMC neurons (SPKO). SPKO mice exhibited significantly increased fat mass, weight of tissues, including sWAT and eWAT, and enlarged the adipocytes size from the age of 5 months compared with those in control mice (Fig. 2a–f). Importantly, knockout SLC7A14 in POMC neurons significantly decreased the levels of p-HSL and p-PKA substrates, the

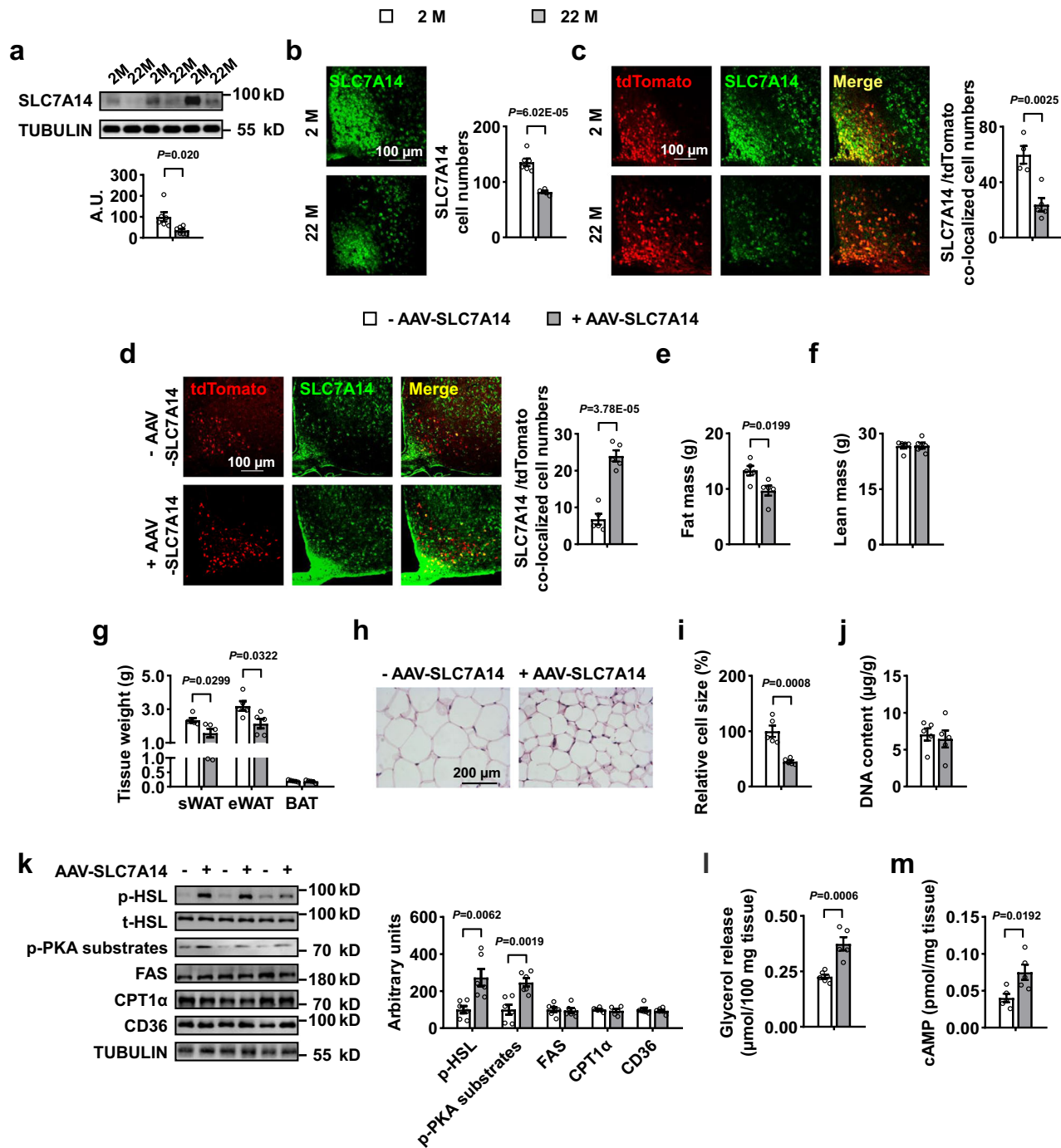


**Fig. 1 | Overexpression of SLC7A14 in POMC neurons is resistant to reduction in lipolysis with age.** **a** SLC7A14 and TUBULIN proteins in hypothalamus. **b** Immunofluorescence (IF) staining for SLC7A14 in ARC sections (left), and quantification of SLC7A14 cell numbers (right). **c**, **d** IF staining for tdTomato, SLC7A14 and merge in ARC sections (left), and quantification of SLC7A14 and tdTomato colocalized cell numbers (right). **e** Fat mass by NMR. **f** Lean mass by NMR. **g** Tissue weight. **h** Representative images of hematoxylin and eosin (H&E) staining of sWAT. **i** Cell size of sWAT quantified by Image J analysis of H&E images. **j** The DNA content of sWAT. **k** p-HSL, t-HSL, p-PKA substrates, FAS, CPT1 $\alpha$ , CD36 and TUBULIN proteins in sWAT by western blotting (left) and quantified by densitometric analysis

(right).  $n = 6$  mice. **l** Glycerol release assays in sWAT. **m** The cAMP levels of sWAT. Studies for **a–c** were conducted using 2-month-old mice (2M) or 22-month-old mice (22M); **d–m** were conducted using 20-month-old POMC Cre mice receiving AAVs expressing mCherry (-AAV-SLC7A14) or SLC7A14 (+AAV-SLC7A14) in ARC. Metabolic tests were performed 1 month after adeno-associated virus injection. For **(a)**,  $n = 6$ . For **(b)**,  $n = 6$  (2M) and 5 (22M). For **(c)**,  $n = 4$  (2M) and 5 (22M). For **(d–j** and **m)**,  $n = 5$ . For **k**,  $n = 6$ . For **l**,  $n = 6$  (-AAV-SLC7A14) and 5 (+AAV-SLC7A14). Data are expressed as the mean  $\pm$  SEM, with individual data points. Data were analyzed by two-tailed unpaired Student's *t*-test (**a–g**, **i–m**). Source data are provided as a Source Data file.

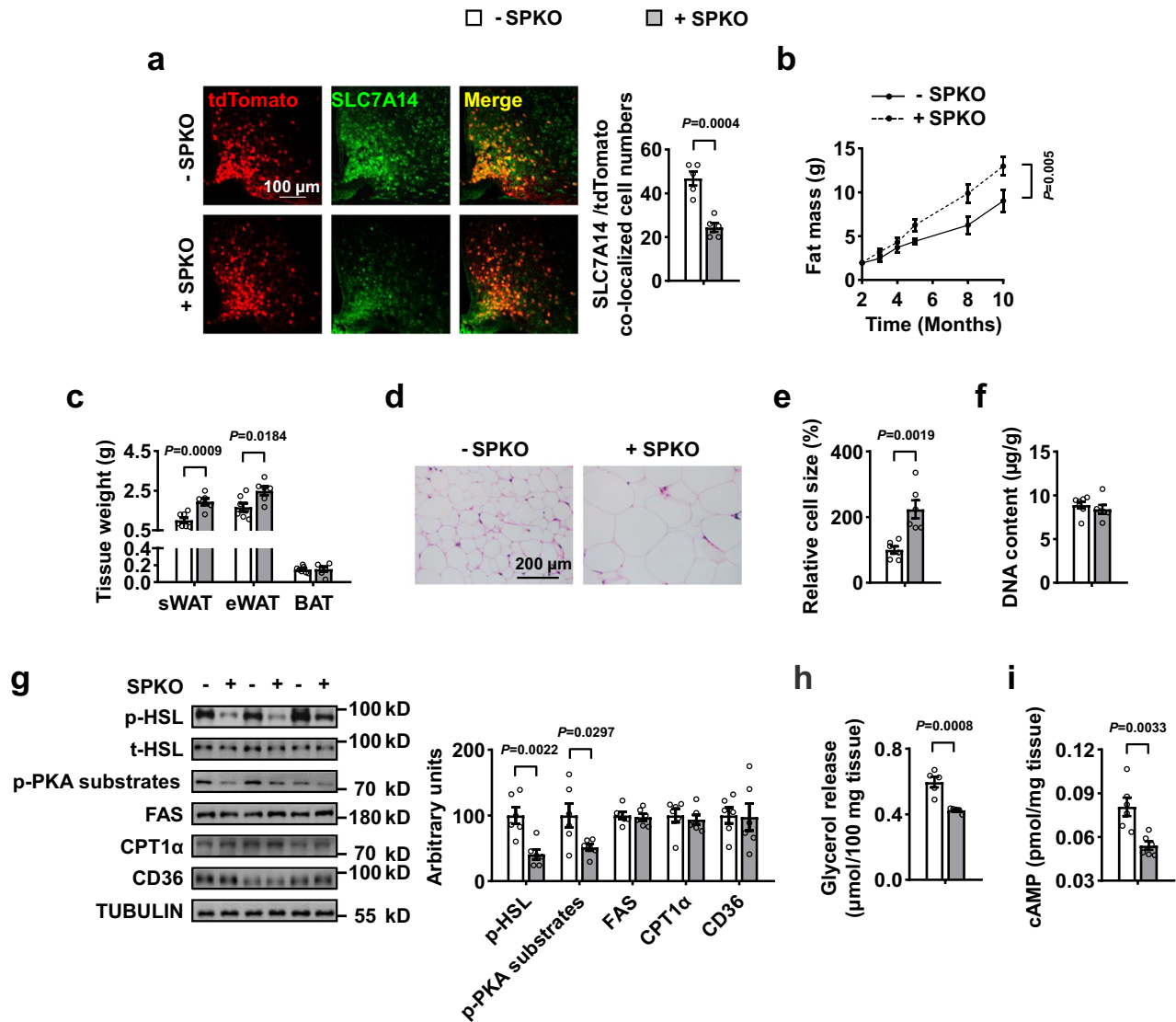


**Fig. 2 | The absence of SLC7A14 in POMC neurons mimics age-induced lipolysis impairment.** **a** IF staining for tdTomato, SLC7A14 and merge in ARC sections (left), and quantification of SLC7A14 and tdTomato colocalized cell numbers (right). **b** Fat mass by NMR. **c** Tissue weight. **d** Representative images of H&E staining of sWAT. **e** Cell size of sWAT quantified by ImageJ analysis of H&E images. **f** The DNA content of sWAT. **g** p-HSL, t-HSL, p-PKA substrates, FAS, CPT1 $\alpha$ , CD36 and TUBULIN proteins in sWAT by western blotting (left) and quantified by densitometric analysis (right). **h** Glycerol release assays in sWAT. **i** The cAMP levels of sWAT. Studies for

(a–i) were conducted using control mice (-SPKO) or mice with SLC7A14 deletion in POMC neurons (+SPKO), and at age of 6-month-old in (a), (c–i). For (a and h),  $n = 5$ . For (b),  $n = 5$  (-SPKO) and 6 (+SPKO). For (c),  $n = 7$  (-SPKO) and 6 (+SPKO). For (d, e, g and i),  $n = 6$ . For (e),  $n = 6$ . For (f),  $n = 7$  (-SPKO) and 6 (+SPKO). Data are expressed as the mean  $\pm$  SEM, with individual data points. Data were analyzed by two-tailed unpaired Student's *t*-test (a, c, e–i), or two-way RM ANOVA with Geisser-Greenhouse's correction (b). Source data are provided as a Source Data file.

glycerol release ability and the cAMP levels in sWAT, which mimicked the age-induced lipolysis impairment (Fig. 2g–i). Furthermore, the expression of UCPI, the cAMP levels, histological analysis in BAT and rectal temperature did not change in SPKO mice (Figs. S5a–e). Additionally, the food intake, oxygen consumption, heat, RER, and locomotor activity did not differ between SPKO and control mice (Figs. S5f–j).

Cold stress has been shown to induce WAT lipolysis<sup>32,33</sup>. To verify the function of POMC SLC7A14 in regulating lipolysis, we investigated lipolysis impairment in SPKO mice under cold exposure. After exposure at 4 °C for 3 h, the control mice displayed smaller adipocytes, increased levels of p-HSL and glycerol release ability in sWAT, but no changes were observed in sWAT of SPKO mice (Figs. S6a–d). Furthermore, enhanced BAT thermogenesis and a decreased rectal temperature were observed in SPKO and control mice under cold exposure (Figs. S6e–h). These results confirm the role of POMC SLC7A14 in regulating WAT lipolysis.

### POMC SLC7A14 regulates lipolysis independently of sympathetic nerves in WAT

Next, we investigated how POMC SLC7A14 regulates WAT lipolysis. Many previous studies have shown that the central nervous system regulates WAT lipolysis by regulating sympathetic nerves in WAT. To assess the essential role of sympathetic nerves in WAT in the lipolysis process, we examined the NE levels in serum, sWAT, eWAT and BAT, and tyrosine hydroxylase (TH) levels in sWAT, and found no difference between SPKO or SPOE mice and their respective control mice (Figs. S7a–f). To further verify the involvement of the sympathetic nerves in WAT in the regulation of lipolysis by POMC SLC7A14, we applied the pharmacotoxic approach of using 6-hydroxydopamine (6-OHDA) to locally ablate the sympathetic fibers in the sWAT of SPOE mice. The ablation of sympathetic nerves in WAT (as reflected by the reduced levels of NE and TH in sWAT) didn't attenuate the effects of POMC SLC7A14-enhanced lipolysis (Figs. S7g–i). These results strongly

suggest POMC SLC7A14 regulates WAT lipolysis independently of sympathetic nerves in WAT.

### POMC SLC7A14 regulates lipolysis via affecting the levels of TCDCA that binds to TGR5

To investigate the mechanisms underlying SLC7A14-increased WAT lipolysis, we performed serum untargeted metabolomics in control and SPOE mice serum. The principal component analysis (PCA) plot with all samples including quality control (QC) samples showed QC samples clustered tightly together, which indicating that data was reliable (Fig. S8a). Additionally, data QC was performed by Pearson correlation analysis to obtain stable and accurate metabolome results. The Pearson correlation QC samples was high, indicating that the data quality was reliable and stable (Fig. S8b). Metabolite set enrichment analysis indicated that the most significant factors were bile acids (Fig. 3a). The levels of tauro- $\alpha$ -muricholic acid (T- $\alpha$ -MCA), 23-norcholeic acid (23-NorCA), glycocholic acid (GCA), cholic acid (CA), and taurochenodeoxycholic acid (TCDCA), which was identified with a metabolomics standards initiative (MSI) level 2 identification (Fig. S8c), were increased in SPOE mice serum. We further confirmed the levels of these bile acids in SPOE mice serum by (high-performance liquid chromatography) HPLC, and found that the TCDCA level increased the most (Fig. 3b and Fig. S8d). Besides, among the five primary bile acids, only TCDCA levels were decreased in the serum of SPKO mice, as evaluated by HPLC (Fig. 3c and Fig. S8e). To investigate a role of TCDCA in the regulation of WAT lipolysis by POMC SLC7A14, we injected control or SPKO mice with phosphate-buffered saline (PBS) or 50 mg/kg TCDCA, and found TCDCA administration rescued SPKO-increased fat mass, weights of sWAT and eWAT, and impaired WAT lipolysis in SPKO mice (Fig. 3d–l and Fig. S8f), but didn't change the expression of UCPI and histological analysis in BAT (Figs. S8g, h). Furthermore, we found TCDCA directly promoted lipolysis of white adipocytes (Fig. 4a, b). It is shown that TCDCA can increase cAMP levels<sup>34</sup>, which is a key upstream of HSL<sup>35</sup>. Thus, we speculated that TCDCA may regulate lipolysis via cAMP. As expected, SQ22536 treatment, a cAMP inhibitor<sup>36</sup>, blocked TCDCA-increased cAMP levels and glycerol release in primary adipocytes (Fig. 4c, d). G protein-coupled bile acid receptor 1 (TGR5) is a G protein-coupled receptor, which expressed in several tissues such as adipose tissues and muscle, where can be activated by bile acids<sup>37</sup>. We found the effect of TCDCA was dependent on TGR5, as shown by the observation showing that knocking down TGR5 in primary adipocytes blocked TCDCA-stimulated the increase in cAMP levels and glycerol release (Fig. 4e–g). Moreover, the increased cAMP levels and glycerol release by INT777, a known TGR5 agonists<sup>37</sup>, was blocked by SQ22536 (Fig. 4h, i). These results strongly suggest that the decreased TCDCA may account for SPKO-impaired WAT lipolysis, and the effect of TCDCA is mediated by upregulating cAMP levels through TGR5.

### ASBT-dependent intestinal bile acid reabsorption determines TCDCA levels regulated by POMC SLC7A14

Next, we explored how POMC SLC7A14 regulates TCDCA levels. The liver is important for synthesizing bile acids<sup>21</sup>. However, the TCDCA levels in the liver of aged SPOE mice did not change (Fig. S9a), nor did the expression of its synthetic genes change in liver of SPOE or SPKO mice (Fig. S9b, c), which suggests POMC SLC7A14 does not regulates TCDCA levels via bile acid synthesis in liver. Surprisingly, we found the levels of TCDCA were significantly increased in the intestine and decreased in the feces of SPOE mice (Fig. 5a, b), which suggested that SLC7A14 might affect the intestinal reabsorption of TCDCA. Furthermore, the expression of the intestinal bile acid reabsorption transporter intestinal apical sodium-dependent bile acid transporter (ASBT) significantly increased in the ileum of SPOE mice (Fig. 5c, d). Consistently, the levels of TCDCA were significantly reduced in the intestines and increased in feces of SPKO mice and aged mice, and the expression of ASBT was significantly decreased in the ileum of SPKO and aged mice

(Fig. 5e–h and Fig. S9d–f). In addition, changes in farnesoid x-activated receptor (FXR) expression in SPOE, SPKO, and aged mice further suggested changes in intestinal TCDCA levels (Fig. S9g–i). To further confirm the role of ASBT in SLC7A14-increased TCDCA content, we used linerixibat, an ASBT inhibitor, to investigated whether inhibition of ASBT block the effect of SLC7A14 on TCDCA levels. As predicted, the promotion of TCDCA levels and WAT lipolysis by SLC7A14 was significantly rescued in SPOE mice injected with linerixibat (Fig. 5i–l). There are studies have reported that PPAR $\alpha$  can activate the promoter of ASBT<sup>38</sup>, so we speculate that POMC SLC7A14 regulate ASBT expression may through PPAR $\alpha$ . We found that the expression of PPAR $\alpha$  was significantly elevated in the ileum of SPOE mice and significantly reduced in the ileum of SPKO and aged mice (Fig. S9j–l). To investigate whether PPAR $\alpha$  is involved in regulating SLC7A14-regulated ASBT expression, we injected SPOE mice with AAVs expressing small-hairpin RNA specific for PPAR $\alpha$  (+AAV-shPPAR $\alpha$ ) or EGFP fluorescent protein (-AAV-shPPAR $\alpha$ ) in ileum (Fig. 5m, n). We found that knockdown of PPAR $\alpha$  blocked POMC SLC7A14-increased ASBT expression (Fig. 5o). Furthermore, we injected SPKO mice with ciprofibrate, a PPAR $\alpha$  activator<sup>39</sup>, and found that activation of PPAR $\alpha$  rescued SLC7A14 knockout-induced decreased ASBT expression (Fig. S9m–n). Next, we explored how POMC SLC7A14 regulate PPAR $\alpha$ . It is shown that oleoylethanolamide (OEA) is an endogenous high-affinity agonist of PPAR $\alpha$ <sup>40</sup>. Therefore, we examined OEA content in the ileum of SPOE or SPKO mice, and found POMC SLC7A14 could regulate OEA levels (Fig. 5p, q). Moreover, supplement of OEA in SPKO mice rescued SLC7A14 knockout-decreased PPAR $\alpha$  expression (Fig. 5r–t). These results strongly indicate that intestinal PPAR $\alpha$ /ASBT mediates the increases in TCDCA levels and WAT lipolysis by POMC SLC7A14.

### POMC SLC7A14 regulates ASBT expression possibly via intestinal sympathetic afferent nerves

Next, we investigated the mechanism underlying the increase in OEA levels, PPAR $\alpha$  and ASBT expression by POMC SLC7A14. Previous studies have shown that intestinal sympathetic afferent nerves can regulate OEA levels. We speculated that the intestinal sympathetic afferent nerves might be involved in the regulation of POMC SLC7A14-increased OEA levels. To investigate whether POMC neurons can project to the intestine, we injected pseudorabies virus (BC-PRV-531-PRV-CAG-EGFP) into the ileum of POMC Cre mice (Fig. 6a), which carrying Ai9 (tdTomato) reporter. After 6 days, a fluorescent signal of the PRV was seen in the celiac ganglion and superior mesenteric ganglion (CG-SMG) and found to be merged with POMC neurons (Fig. 6b, c), indicating that POMC neurons can potentially deliver information to the ileum through intestinal sympathetic afferent nerves. Furthermore, we found that the protein levels and immunofluorescence of TH and NE levels were decreased in intestine of SPKO mice (Fig. 6d–f). Consistently, the protein levels and immunofluorescence of TH and NE levels were increased in intestine of SPOE mice (Fig. 6g–i). To assess the essential role of intestinal sympathetic afferent nerves in POMC SLC7A14 regulating OEA levels, PPAR $\alpha$  and ASBT expression, CG-SMG ganglionectomy was performed in SPOE mice. As predicted, the removal of the CG-SMG blocked SLC7A14-promoted intestinal OEA levels, PPAR $\alpha$  and ASBT expression and serum TCDCA levels (Fig. 6j–q). Furthermore, SPOE mice were injected with propranolol, a  $\beta$ -adrenergic receptor inhibitor<sup>41</sup>, and blocked POMC SLC7A14-promoted OEA levels, PPAR $\alpha$  and ASBT expression (Fig. S9o–q). These results strongly suggest that intestinal sympathetic afferent nerves are involved in the regulation of ASBT expression and TCDCA levels by POMC SLC7A14.

### SLC7A14 regulates intestinal sympathetic afferent nerves through POMC mTORC1 signaling

Next, we explored the signaling pathway that mediate the effects of in POMC SLC7A14 on intestinal sympathetic afferent nerves. Previous

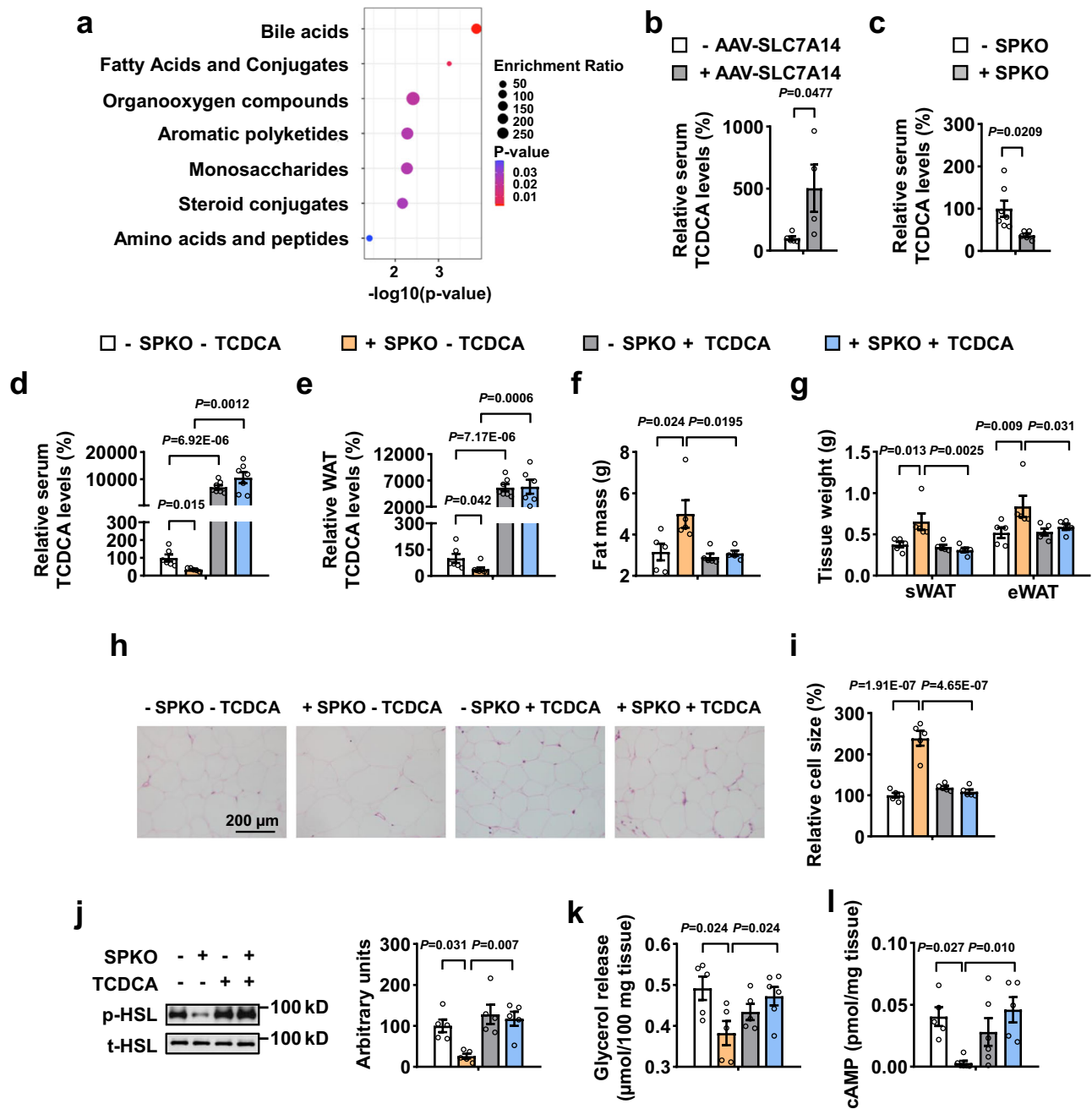


**Fig. 3 | The decreased TCDCDA mediates SPKO-induced WAT lipolysis impairment.** **a** Metabolite set enrichment analysis. **b–d** The TCDCDA levels of serum. **e** The TCDCDA levels of WAT. **f** Fat mass by NMR. **g** Tissue weight. **h** Representative images of H&E staining of sWAT. **i** Cell size of sWAT quantified by Image J analysis of H&E images. **j** p-HSL and t-HSL proteins in sWAT. **k** Glycerol release assays in sWAT. **l** The cAMP levels of sWAT. Studies for **a** and **b** were conducted using 20-month-old POMC Cre mice receiving AAVs expressing mCherry (-AAV-SLC7A14) or SLC7A14 (+AAV-SLC7A14) in ARC. **c–l** were conducted using 5-month-old control mice (-SPKO) or mice with SLC7A14 deletion in POMC neurons (+SPKO). Mice were intraperitoneally (i.p.) injected with PBS (-TCDCA) or 50 mg/kg body weight TCDCA (+TCDCA) every other day. On the fifteenth day, mice were i.p. injected with a single

dose of TCDCA before euthanized in (**d–l**). For (**a**, **b**),  $n=5$  (- AAV-SLC7A14) and 4 (+AAV-SLC7A14). For (**c**),  $n=7$  (- SPKO) and 4 (+SPKO). For (**d**),  $n=6$  (- SPKO - TCDCA), 5 (+SPKO - TCDCA), 7 (- SPKO + TCDCA) and 7 (+SPKO + TCDCA). For (**e**),  $n=6$  (- SPKO - TCDCA), 7 (+SPKO - TCDCA), 7 (- SPKO + TCDCA) and 6 (+SPKO + TCDCA). For (**f** and **h–j**),  $n=5$ . For (**g**),  $n=6$ . For **k**,  $n=5$  (-SPKO - TCDCA), 5 (+SPKO - TCDCA), 6 (-SPKO + TCDCA) and 6 (+SPKO + TCDCA). For **l**,  $n=5$  (-SPKO - TCDCA), 6 (+SPKO - TCDCA), 6 (- SPKO + TCDCA) and 5 (+SPKO + TCDCA). Data are expressed as the mean  $\pm$  SEM, with individual data points. Data were analyzed by Fisher's exact test (**a**) or two-tailed unpaired Student's *t*-test (**b**, **c**), or ordinary two-way ANOVA with Tukey's multiple comparisons test (**d–g**, **i–l**). Source data are provided as a Source Data file.

study has shown that POMC mTOR signaling plays an important role in age-dependent obesity<sup>3,9</sup>. Because mTORC1 activity is regulated at lysosome, where SLC7A14 is localized<sup>28</sup>, we speculated that mTORC1 might be involved in the regulatory effect of SLC7A14. As predicted, SLC7A14 could regulate mTORC1 signaling and activity in primary hypothalamic cells (Fig. 7a–d), and p-S6 levels were significantly

decreased in POMC neurons of SPKO mice (Fig. 7e). To further clarify the role of POMC mTORC1 signaling in SLC7A14-regulated intestinal sympathetic afferent nerves, SPKO mice were injected with Cre dependent AAVs expressing small-hairpin RNA specific for RAPTOR (+AAV-shRAPTOR) or mCherry fluorescent protein (-AAV-shRAPTOR) in POMC neurons (Fig. 7f). Knockdown of RAPTOR rescued the effects

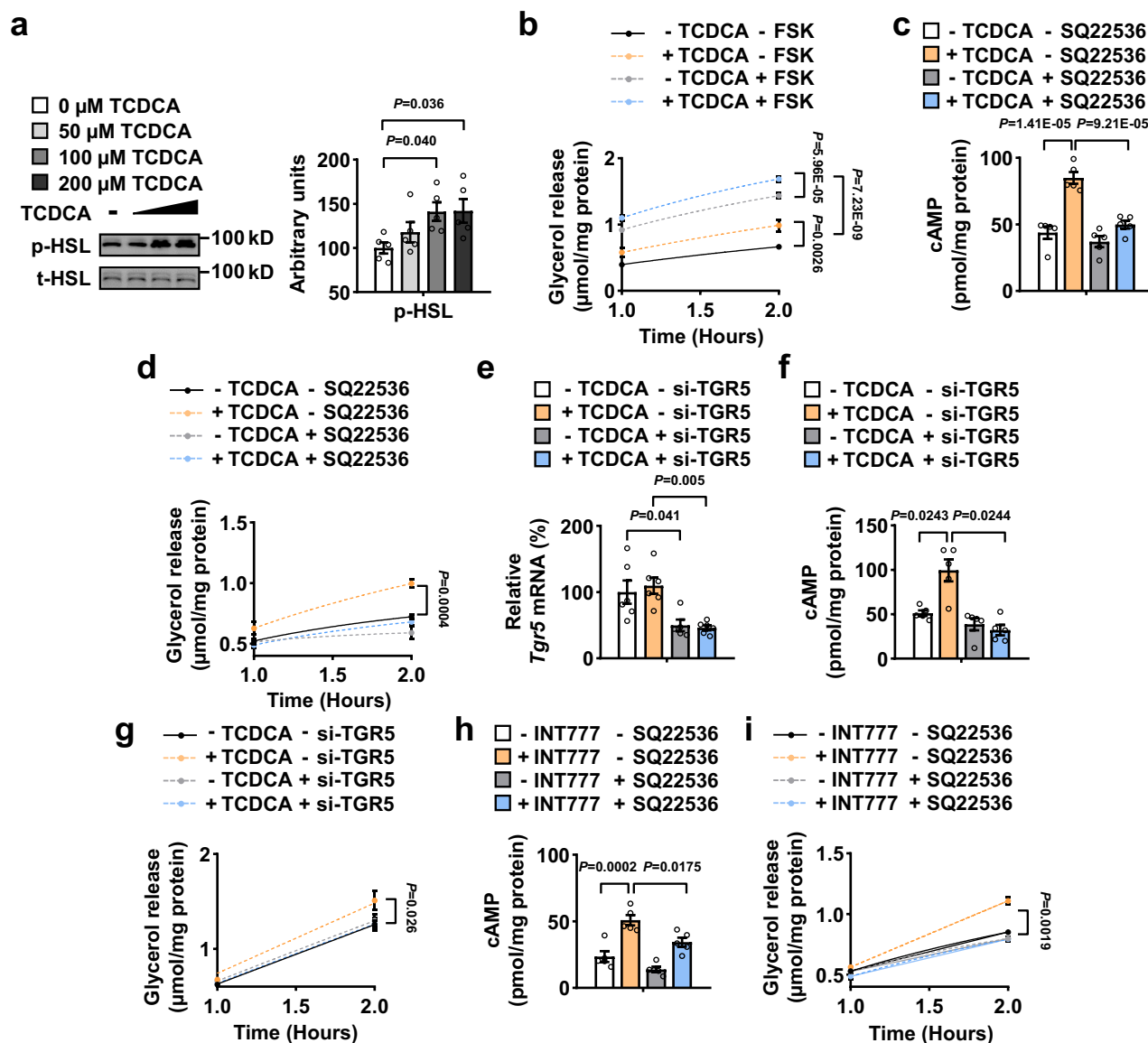


**Fig. 4 | TGR5 mediates TCDC A-stimulated lipolysis via regulating cAMP levels.**

**a** P-HSL and t-HSL proteins in primary white adipocytes. **b, d, g** and **i** Glycerol release assays in primary white adipocytes. **c, f** and **h** The cAMP levels of primary white adipocytes. **e** The mRNA levels of TGR5 in primary white adipocytes. Studies for **a** were conducted using primary white adipocytes treated with control vehicle (-TCDC A) or TCDC A (+TCDC A) at the concentration as indicated for 4 h. **b** Were conducted using primary white adipocytes treated with control vehicle (-TCDC A) or 100 μM TCDC A (+TCDC A) for 2 h, followed by incubation with Krebs-Ringer buffer, with or without 10 μM FSK, with or without 100 μM TCDC A at 37 °C for 2 h. **c, d** were conducted using primary white adipocytes treated with or without 100 μM TCDC A in the presence or absence of 100 μM SQ22536 for 4 h; **e-g** were conducted using primary white adipocytes transfected with double-stranded siRNA

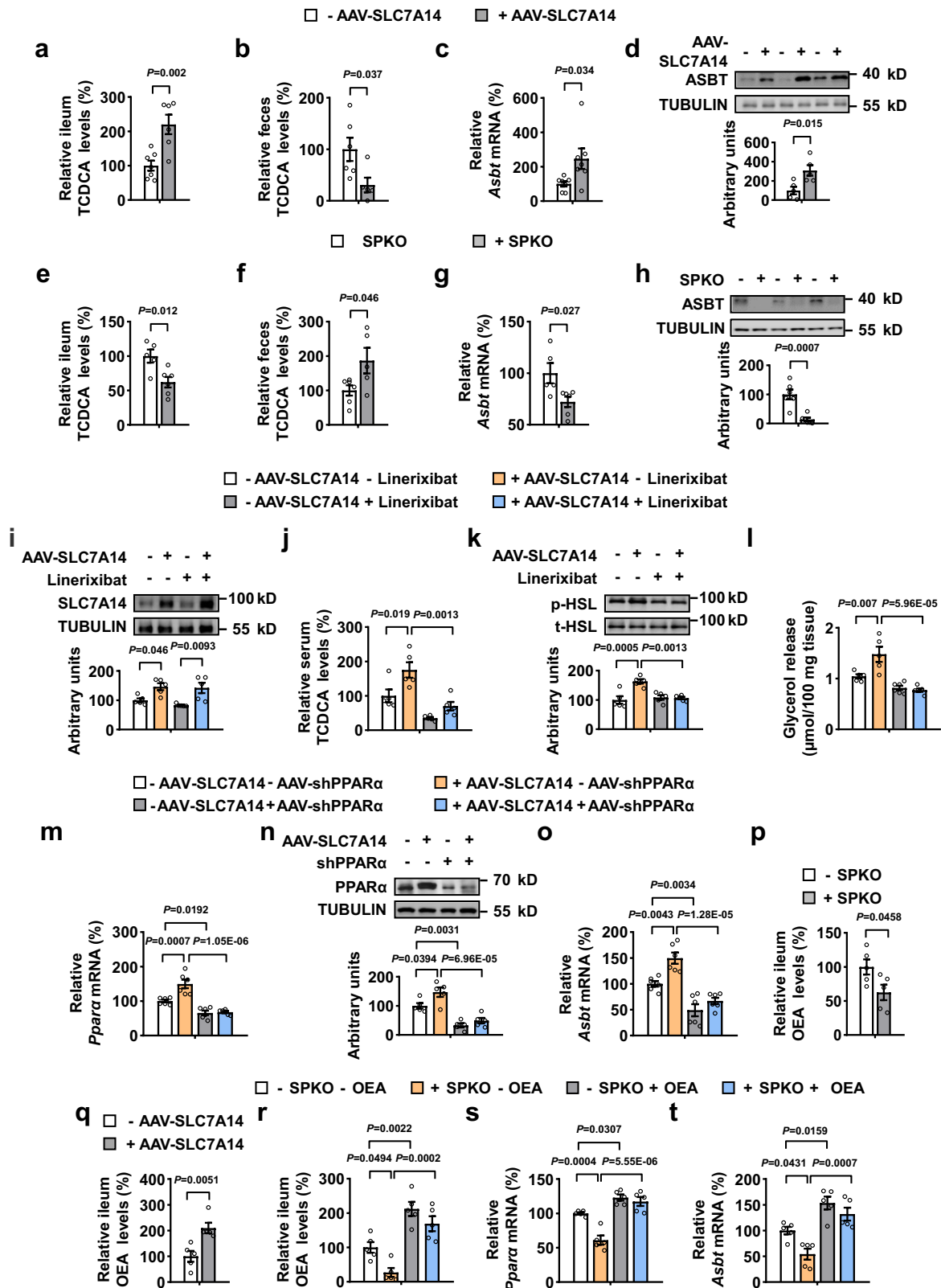
targeting TGR5 for 72 h, followed by treating with control vehicle (-TCDC A) or 100 μM TCDC A (+TCDC A) for 4 h; **h, i** were conducted using primary white adipocytes treated with or without 30 μM INT777 in the presence of control vehicle or 100 μM SQ22536 for 2 h. For (**a, c, d, f, h** and **i**),  $n = 5$ . For (**b**),  $n = 7$  (-TCDC A - FSK), 6 (+TCDC A - FSK), 6 (-TCDC A + FSK) and 5 (+TCDC A + FSK). For (**e**),  $n = 6$  (-TCDC A - siTGR5), 6 (+TCDC A - siTGR5), 5 (-TCDC A + siTGR5) and 6 (+TCDC A + siTGR5). For (**g**),  $n = 6$  (-TCDC A - siTGR5), 5 (+TCDC A - siTGR5), 5 (-TCDC A + siTGR5) and 6 (+TCDC A + siTGR5). Data are expressed as the mean  $\pm$  SEM, with individual data points. Data were analyzed by ordinary one-way ANOVA with Dunnett's multiple comparisons test (**a**), or two-way RM ANOVA with Geisser-Greenhouse's correction (**b, d, g, i**) or ordinary two-way ANOVA with Tukey's multiple comparisons test (**c, e, f, and h**). Source data are provided as a Source Data file.

of POMC SLC7A14 knockout on the parameters examined, except for lean mass that was not changed in any case (Fig. 7g-l). These results strongly suggest that POMC SLC7A14-induced intestinal sympathetic afferent nerves changes are regulated by POMC mTORC1 signaling.

#### POMC SLC7A14 regulates mTORC1 signaling via TSC1

Next, we investigated the underlying mechanism of the inhibition of the mTORC1 signaling pathway by POMC SLC7A14. TSC1 is a known repressor of the mTORC1 signaling pathway<sup>42</sup>. Previous studies have reported IKK $\beta$ , which was activated in hypothalamus of aging mice<sup>22</sup>, phosphorylated TSC1 on Ser511<sup>26</sup>, thereby stimulated

mTORC1 signaling pathway. We found that the overexpression of SLC7A14 inhibited the phosphorylation of TSC1 at Ser511, whereas SLC7A14 knockdown had the opposite effect (Fig. 8a, b and Fig. S10a, b). Moreover, SPOE mice were injected with Cre dependent AAVs expressing small-hairpin RNA specific for TSC1 (+AAV-shTSC1) or mCherry fluorescent protein (-AAV-shTSC1) in POMC neurons (Fig. S10c). Knockdown of TSC1 blocked POMC SLC7A14-increased activation of intestinal sympathetic afferent nerves, intestinal PPAR $\alpha$  and ASBT expression and glycerol release in WAT (Fig. S10d-h). To further confirm the role of TSC1 in the inhibition of the mTORC1 signaling pathway by SLC7A14, primary hypothalamic cells,



which were infected with Ad-SLC7A14, were transfected plasmid expressing small-hairpin RNA specific for TSC1. Knockdown of TSC1 reversed the inhibition of the mTORC1 signaling pathway by SLC7A14, suggesting that TSC1 mediated the regulation of mTORC1 signaling by SLC7A14 (Fig. 8c). IKK $\beta$  is a known regulator of p-TSC1 ser511<sup>26</sup>, and activated in hypothalamus of aging mice<sup>22</sup>. We speculated that SLC7A14 was involved in the regulation of TSC1 phosphorylated

by IKK $\beta$ . As predicted, overexpression of SLC7A14 blocked IKK $\beta$ -enhanced p-TSC1 ser511 (Fig. 8d). Moreover, we found SLC7A14 suppressed p-TSC1 ser511 may through inhibiting interaction between IKK $\beta$  and TSC1 (Fig. 8e). Next, we explored how SLC7A14 inhibited the IKK $\beta$  and TSC1 interaction. We used HitPredict<sup>43</sup>, a widely used database with quality assessed protein-protein interactions, to assess protein interactions of SLC7A14, IKK $\beta$  or TSC1. Further analysis showed that



**Fig. 5 | The intestinal ASBT mediates POMC SLC7A14-induced TCDC levels and WAT lipolysis.** **a** and **e** The TCDC levels of ileum. **b** and **f** The TCDC levels of feces. **c, g, o** and **t** The mRNA levels of *Asbt* in ileum by RT-PCR. **d** and **h** ASBT and TUBULIN proteins in ileum. **i** SLC7A14 and TUBULIN proteins in ARC. **j** The TCDC levels of serum. **k** P-HSL and t-HSL proteins in sWAT. **l** Glycerol release assays in sWAT. **m** and **s** The *Ppar $\alpha$*  mRNA levels in ileum by RT-PCR. **n** PPAR $\alpha$  and TUBULIN proteins in ileum. **p–r** The OEA levels of ileum. Studies for a–d, q and i–o were conducted using POMC Cre mice receiving AAVs expressing mCherry (- AAV-SLC7A14) or SLC7A14 (+AAV-SLC7A14) in ARC, and treated twice daily with control vehicle (- linerixibat) or 0.05 mg/kg linerixibat (+ linerixibat) via oral gavage in i–l, or the ileum of mice was injected with AAVs expressing shPPAR $\alpha$  (+ AAV-

shPPAR $\alpha$ ) or EGFP (-AAV-shPPAR $\alpha$ ) in **m–o**. **e–h, p** and **r–t** were conducted using 6-month-old control mice (- SPKO) or mice with SLC7A14 deletion in POMC neurons (+ SPKO), and mice were given OEA (10 mg/kg, aladdin) in (**r–t**). For **a**,  $n = 7$  (- AAV-SLC7A14) and 6 (+AAV-SLC7A14). For **b**,  $n = 6$  (- AAV-SLC7A14) and 5 (+AAV-SLC7A14). For (**c**),  $n = 7$ . For (**d, i–k, n**, and **p–t**),  $n = 5$ . For **e** and **g**,  $n = 5$  (- SPKO) and 6 (+SPKO). For (**f**),  $n = 6$  (- SPKO) and 5 (+SPKO). For (**h**) and **m–o**,  $n = 6$ . For **l**,  $n = 5$  (- AAV-SLC7A14 - Linerixibat), 5 (+AAV-SLC7A14 - Linerixibat), 6 (- AAV-SLC7A14 + Linerixibat) and 5 (+AAV-SLC7A14 + Linerixibat). Data are expressed as the mean  $\pm$  SEM, with individual data points. Data were analyzed by two-tailed unpaired Student's *t*-test (**a–h, p, q**), or ordinary two-way ANOVA with Tukey's multiple comparisons test (**i–o, r–t**). Source data are provided as a Source Data file.

SLC7A14, IKK $\beta$  and TSC1 all interacted with DERL1 (Fig. 8f), which was known to regulate mTORC1 signaling pathway<sup>44</sup>. We further confirmed that DERL1 could interact with SLC7A14, IKK $\beta$  and TSC1 by co-immunoprecipitation (Fig. 8g). Furthermore, we found that over-expression of SLC7A14 inhibited interaction between DERL1 and IKK $\beta$  (Fig. 8h). These results suggesting that SLC7A14 inhibited mTORC1-signaling pathway may through inhibiting interaction between DERL1 and IKK $\beta$ , then suppressing IKK $\beta$  and TSC1 interaction, thereby inhibiting phosphorylation of TSC1.

## Discussion

Aging has an important correlation with obesity<sup>4,5</sup>. With the increase of global aging, there is an urgent need to study age-dependent obesity. Previous studies have reported that impaired lipolysis of adipocytes is an important factor for age-dependent obesity<sup>4,5,8</sup>. Many factors account for the reduction in lipolysis with age. Currently, most studies indicate that the surrounding environment of adipose tissue plays an important role in age-induced lipolysis impairment<sup>4,5,8</sup>. Previous studies have found the central hypothalamic mTOR pathway plays an important role in the regulation of age-dependent obesity<sup>9</sup>, however, the underlying molecular mechanism remains unclear. In addition, the CNS regulates WAT lipolysis mainly through sympathetic nervous system in WAT<sup>12,14</sup>. Some studies have suggested that WAT lipolysis is regulated via other mechanisms<sup>17–19,45</sup>. However, it is currently unclear whether and how the CNS regulates WAT lipolysis through metabolites. SLC7A14 is a lysosomal membrane protein that is highly expressed in the hypothalamus<sup>28</sup>, but its role in regulating lipid metabolism is unclear. In this study, we found that the expression of POMC SLC7A14 are reduced that leading to the activation of mTORC1 during ageing. This generates a sympathetic signal that reduces the expression of ASBT in enterocytes and the subsequent reabsorption of TCDC. TCDC then induces WAT lipolysis via TGR5. Furthermore, we identified the underlying mechanism of the regulation of the mTORC1 signaling pathway by SLC7A14. These results will deepen the understanding of the physiological function of SLC7A14 and may help reveal the molecular mechanisms of age-dependent obesity. This study helps understand the upstream mechanism of the mTORC1 signaling pathway.

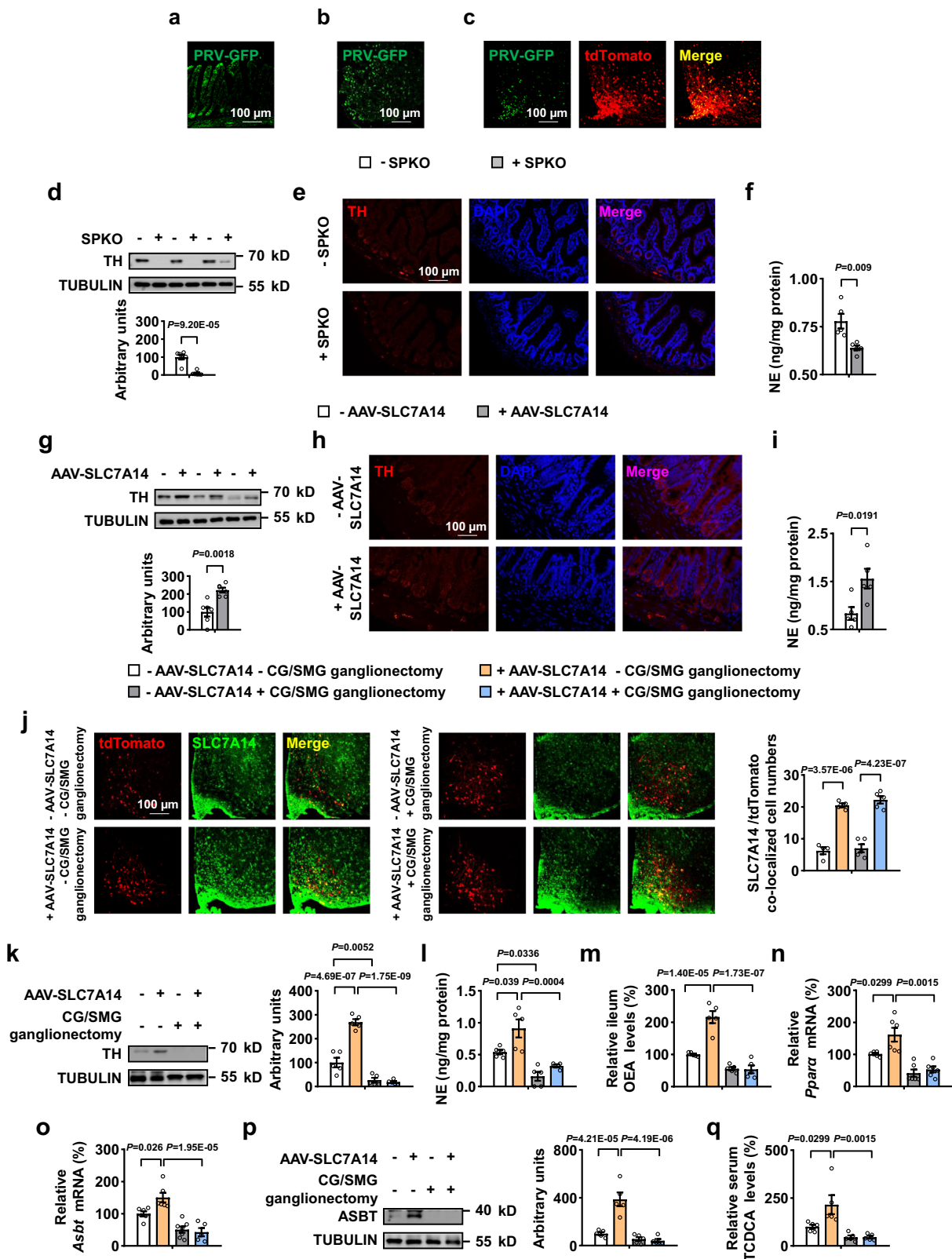
Previous studies have shown that direct regulation of POMC neuronal activity modulates WAT lipolysis via SNS<sup>12</sup>. However, we detected sympathetic nervous activity in WAT and found no differences between SPKO or SPOE mice and their respective control mice. Ablation of sympathetic nerves in WAT had no effect on SLC7A14-enhanced lipolysis. This is an interesting finding as few studies have shown CNS regulated WAT lipolysis independently of SNS in WAT. Recent studies have reported a remarkable degree of heterogeneity in POMC neurons and distinct POMC neurons have distinct function<sup>46</sup>. Thus, POMC neurons expressing SLC7A14 regulate WAT lipolysis may through other pathways besides SNS in WAT. There are some studies have shown that CNS can regulate lipolysis through inflammatory factor or hormone, without relying on the SNS in WAT<sup>17–19</sup>. In our study, we effectively demonstrated that the CNS can regulate lipolysis through metabolites. Bile acids are metabolites

whose production is reduced during aging, and they are known to regulate WAT lipolysis<sup>21</sup>. The levels of bile acids are mainly regulated by the liver, gallbladder, and intestine<sup>21</sup>. Surprisingly, in our study, we found that CNS could regulate bile acids levels. Previous studies have reported that bile acids, especially secondary bile acids, can regulate WAT lipolysis<sup>21</sup>. However, whether the primary bile acid TCDC can regulate lipolysis is still unclear. Furthermore, we showed that the TCDC stimulated lipolysis in WAT through TGR5, but not stimulated BAT thermogenesis. There are other BA-responsive receptors respond to bile acid stimulation and exert different effects in various tissues and cell types<sup>21</sup>. TCDC had no effect on BAT thermogenesis, possibly due to the role of other BA-responsive receptors, except TGR5, in brown adipose tissue. Our data effectively demonstrated that POMC neurons regulated lipolysis through TCDC, which is a new way of regulating lipolysis and a different mode of upstream regulation of bile acids. These findings expand the understanding of central regulation of lipolysis and lay a theoretical foundation for the study of bile acid regulation.

Although current research on brain-gut axis is less-well understood, emerging evidence suggests that CNS can regulate intestinal sympathetic afferent nerves<sup>47</sup>. Besides, previous studies have shown that intestinal sympathetic afferent nerves can regulate intestinal absorption<sup>48</sup>. In our study, we demonstrated that POMC SLC7A14 regulates WAT lipolysis via regulating TCDC levels, which was regulated by ASBT. Furthermore, the study showed that the intestinal sympathetic afferent nerves was involved in the regulation of intestinal bile acid absorption by POMC SLC7A14. This is an important finding, as POMC neurons have a role in regulating intestinal sympathetic afferent nerves and intestinal bile acid absorption. These results provide insights into the brain-gut-adipose tissue crosstalk.

Several studies have shown that POMC mTORC1 signaling pathway accounts for age-dependent obesity<sup>3,9</sup>. In this study, we found that SLC7A14 inhibited the mTORC1 signaling pathway may via inhibiting interaction between DERL1 and IKK $\beta$ , then suppressing IKK $\beta$  and TSC1 interaction, thereby inhibiting phosphorylation of TSC1. A previous study has reported hypothalamic IKK $\beta$  is activated in aged mice<sup>22</sup>. IKK $\beta$  is known to phosphorylation of TSC1<sup>26</sup>, which is an inhibitor of mTORC1<sup>42</sup>. Thus, POMC IKK $\beta$  may has a role in age-dependent obesity via TSC1. A previous study has shown that knockout of TSC1 in POMC neurons, not in AgRP neurons, leads to obesity, which is consistent with the effects of SLC7A14 in POMC and AgRP neurons<sup>9</sup>. Regarding how SLC7A14 regulate mTORC1, there are other possibilities. Such as SLC7A14 inhibits mTORC1 signaling pathway may through regulating lysosomal translocation of TSC1, and/or via its transport function. However, more evidence will be need to support these possibilities. These results reveal the underlying mechanisms of the regulation of mTORC1 by SLC7A14, help understand the upstream mechanism of the mTORC1 signaling pathway, and provide a new role for POMC mTORC1 in regulating intestinal sympathetic afferent nerves.

There are some limitations to this study. First, it is unclear how POMC neuron projects to intestine. The rostral ventrolateral medulla (RVLM) presumably transmits descending sympathetic signals to the



CG-SMG<sup>48</sup>, which suggests that POMC SLC7A14 may regulate the intestinal sympathetic afferent nerves via the projection to RVLM. Second, it is still unclear how inhibiting the interaction between DERL1 and IKK $\beta$  suppresses the IKK $\beta$  and TSC1 interaction. More extensive studies will be required to clarify this point.

Taken together, this study demonstrates an important role for SLC7A14/mTORC1 signaling in POMC neurons in regulating

age-induced reduction in lipolysis (Fig. 8i). Our findings show that POMC SLC7A14/mTORC1 signaling regulates lipolysis through TCDC4, without relying on the SNS in WAT, which is a new way of central regulation of lipolysis and upstream regulation of bile acids. Furthermore, the findings reveal the underlying mechanisms of the regulation of mTORC1 by SLC7A14. These results expand the understanding of the regulation of age-induced lipolysis impairment

**Fig. 6 | POMC SLC7A14 regulates ASBT expression via intestinal sympathetic afferent nerves.** **a** Representative micrographs of the ileum wall demonstrating neurons expressing PRV. **b** Representative micrographs of the CG-SMG demonstrating neurons expressing PRV. **c** Representative micrographs of the brain demonstrating neurons expressing PRV, tdTomato and merge. **d–g, k** TH and TUBULIN proteins in ileum. **e–h** IF staining for DAPI, TH and merge in ileum. **(f, i and l)** The NE levels of ileum. **j** IF staining for tdTomato, SLC7A14 and merge in ARC. **m** The OEA levels of ileum. **n** The *Ppara* mRNA levels in ileum. **o** The *Asbt* mRNA levels in ileum. **p** ASBT and TUBULIN proteins in ileum. **q** The TCDC levels of serum. Studies for a–c were conducted using 5-month-old POMC Cre mice, which carrying Ai9 (tdTomato) reporter, injected with pseudorabies virus (BC-PRV-531-PRV-CAG-EGFP) for 6 days in ileum. **d–f** were conducted using 5-month-old control mice (-SPKO) or mice with SLC7A14 deletion in POMC neurons (+SPKO); **(g–i, j–q)**

were conducted using 20 month-old POMC Cre mice receiving AAVs expressing mCherry (-AAV-SLC7A14) or SLC7A14 (+AAV-SLC7A14) in ARC, and treated with sham surgery (-CG/SMG ganglionectomy) or surgical removal of celiac-superior mesenteric ganglion (+CG/SMG ganglionectomy) in j–q. For a–c, n = 7. For **(d–g, n)** n = 6. For **(e)** and **(h)** n = 3. For **(f–i, k–m)** and **(p–q)** n = 5. For **(j)** n = 4 (-AAV-SLC7A14 -CG/SMG ganglionectomy), 4 (+AAV-SLC7A14 -CG/SMG ganglionectomy), 5 (-AAV-SLC7A14 +CG/SMG ganglionectomy) and 5 (+AV-SLC7A14 +CG/SMG ganglionectomy). For **(o)** n = 6 (-AAV-SLC7A14 -CG/SMG ganglionectomy), 6 (+AAV-SLC7A14 -CG/SMG ganglionectomy), 7 (-AAV-SLC7A14 +CG/SMG ganglionectomy) and 5 (+AAV-SLC7A14 +CG/SMG ganglionectomy). Data are expressed as the mean ± SEM, with individual data points. Data were analyzed by two-tailed unpaired Student's *t*-test **(d–f, g–i)** or ordinary two-way ANOVA with Tukey's multiple comparisons test **(j–q)**. Source data are provided as a Source Data file.

by the brain–gut–adipose tissue axis, provide insights into upstream regulation of bile acids.

## Methods

### Animals and treatments

All mice experiments were approved by the guidelines of the Institutional Animal Care and Use Committee at Fudan University (ethical committee approval no.2022030006 S) and the Shanghai Institute of Nutrition and Health, Chinese Academy of Sciences (ethical committee approval nos. SINH-2020-GFF-1, SINH-2021-GFF-1 and SINH-2022-GFF-1). All mice used were male and of a C57BL/6J background. Two month or 6 month or 22 old month aged male C57BL/6J mice were used for experiments. Wild-type (WT) mice were obtained from the Model Animal Research Center of Nanjing University (Nanjing, China). POMC-Cre mice were provided by Joel K. Elmquist and Tiemin Liu from the Southwestern Medical Center. POMC neuron-specific SLC7A14 knockout (SPKO) mice were generated by crossing SLC7A14 *flax/flax* mice (MARC, Nanjing, China) with POMC-Cre mice. Ai9 (tdTomato) reporter mice, which is Cre-driver lines for cell-type-specific genetic manipulation, were obtained from the Jackson Laboratory. To visualize POMC protein-expressing neurons under the fluorescence microscope, SPKO and POMC-Cre mice were intercrossed with Ai9 reporter mice. Mice were housed on a 12 h light/dark cycle from 7 A.M. to 7 P.M. at room temperature (25 °C) and provided free access to standard

chow rodent diets (Shanghai Pu Lu Teng Biotechnology, P1103F) and water. Mice were sacrificed by CO<sub>2</sub> inhalation. For acute cold exposure studies, 5-month-old SLC7A14 *flax/flax* mice or SPKO mice were caged individually and exposed at 4 °C in the absence of food, water or bedding, while control mice received the same treatment at 25 °C. For TCDC treatment, mice were intraperitoneally (i.p.) injected with TCDC (50 mg/kg body weight; MCE) every other day. On the 15th day, mice were i.p. injected with a single dose of TCDC (50 mg/kg body weight, MCE) before euthanized. For linerixibat treatment, mice were given linerixibat (0.05 mg/kg, MCE), which was dissolved in 0.5% hydroxypropyl methylcellulose, 0.1% Tween80 and 0.5% dimethyl sulfoxide, via oral administration twice a day (9.00 a.m. and 6.00 p.m.) for three consecutive days. On the 4th day, mice were given a single dose of linerixibat before euthanized. For OEA treatment, mice were given OEA (10 mg/kg body weight, aladdin), which was dissolved in 5% Tween80 saline, via i.p. injection once daily for 2 weeks. On the 15th day, mice were given a single dose of OEA before euthanized. For ciprofibrate treatment, mice were given ciprofibrate (10 mg/kg, MCE), via oral administration once daily for 1 weeks. On the 8th day, mice were given a single dose of ciprofibrate before euthanized. For (S)-(-)-Propranolol hydrochloride (1 mg/kg, aladdin) treatment, mice were given (S)-(-)-Propranolol hydrochloride via i.p. injection for 30 min.

### Stereotaxic surgery and viral injections

Stereotaxic surgeries were performed on the mice with a stereotaxic frame (Steolting, IL, USA)<sup>49</sup>. The mice were bilaterally injected virus into

ARC (1.58 mm posterior to the bregma, ±0.25 mm lateral to the midline, and 5.9 mm below the surface of the skull). Mice were i.p. injected with antibiotics (ceftriaxone sodium, 0.1 g/kg) intraperitoneally for 2 days to prevent infection. After the surgery, the mice recovered for at least 3–4 weeks before conducting the experiments.

To knock down of SLC7A14 in ARC, SLC7A14 *flax/flax* mice were bilaterally injected either with an AAV vector containing Cre recombinase (AAV9-CAG-EGFP-P2A-Cre-WPRE, 3.84 × 10<sup>12</sup> v.g/mL, OBio technology) at a volume of 200 nL into the ARC or with an AAV vector containing only EGFP (AAV9-CAG-EGFP-P2A-MCS-WPRE, 3.84 × 10<sup>12</sup> v.g/mL, OBio technology) as a control.

To overexpression of SLC7A14 in ARC POMC neurons, POMC Cre mice were bilaterally injected either with a Cre-dependent AAV vector containing SLC7A14 in the opposite orientation flanked by two inverted loxP sites (AAV9-Syn-DIO-SLC7A14-mCherry, 1.5 × 10<sup>12</sup> v.g/mL, Hanbio Tech) at a volume of 200 nL into the ARC or an AAV vector containing only mCherry in the opposite orientation flanked by two inverted loxP sites (AAV9-Syn-DIO-mCherry, 1.5 × 10<sup>12</sup> v.g/mL, Hanbio Tech) as a control.

To assess whether the suppression of RAPTOR in POMC neurons could reverse the effect of POMC SLC7A14 knockout on intestinal sympathetic nervous system, POMC Cre mice or SPKO mice were bilaterally injected either with a Cre-dependent AAV vector containing mir-30-shRaptor coding sequence and mCherry protein in the opposite orientation flanked by two inverted loxP sites (AAV9-CMV-DIO-mir-30-shRAPTOR-GFP, 1.5 × 10<sup>12</sup> v.g/mL, Hanbio Tech) at a volume of 200 nL into the ARC, or an AAV vector containing the mir-30-scramble and mCherry protein in the opposite orientation flanked by two inverted loxP sites (AAV9-CMV-DIO-mir-30-scramble-GFP, 1.5 × 10<sup>12</sup> v.g/mL, Hanbio Tech) as a control. The 5'-GGACAA CGGTCACAAGTACTT-3' was the target sequence for RAPTOR.

To assess whether the suppression of TSC1 in POMC neurons could reverse the effect of POMC SLC7A14 overexpression on mTORC1 signaling and intestinal sympathetic nervous system, POMC Cre mice were bilaterally injected either with Cre-dependent AAVs expressing SLC7A14 (AAV9-Syn-DIO-SLC7A14-mCherry, 1.5 × 10<sup>12</sup> v.g/ml, Hanbio Tech), shTSC1 (AAV9-CMV-DIO-mir-30-shTSC1-ZsGreen, 1.5 × 10<sup>12</sup> v.g/ml, Hanbio Tech), as well as control AAVs expressing mCherry (AAV9-Syn-DIO-mCherry, 1.5 × 10<sup>12</sup> v.g/mL, Hanbio Tech) or GFP (AAV9-CMV-DIO-mir-30-Scramble-ZsGreen), as indicated. The 5'-TTGTACATCCGTATAGTAA-3' was the target sequence for TSC1.

### Ileal AAV injections

Mice were anesthetized. After shaving and sterilization of the abdomen, mice were placed on a sterile surgical pad and covered with a sterile surgical drape. The ileum was exposed by making a midline incision through the abdominal wall. The ileum of mice was injected with 10 μL AAVs expressing shPPARα (AAV2/9-U6-shPPARα-CMV-EGFP, 1 × 10<sup>12</sup> v.g/ml, Hanbio Tech) or EGFP (AAV2/9-U6-MCS-CMV-EGFP, 1 × 10<sup>12</sup> v.g/ml, Hanbio Tech) as a control. The 5'-TCACACAATGCAATTCGCTTTGGA-3' was the target sequence for

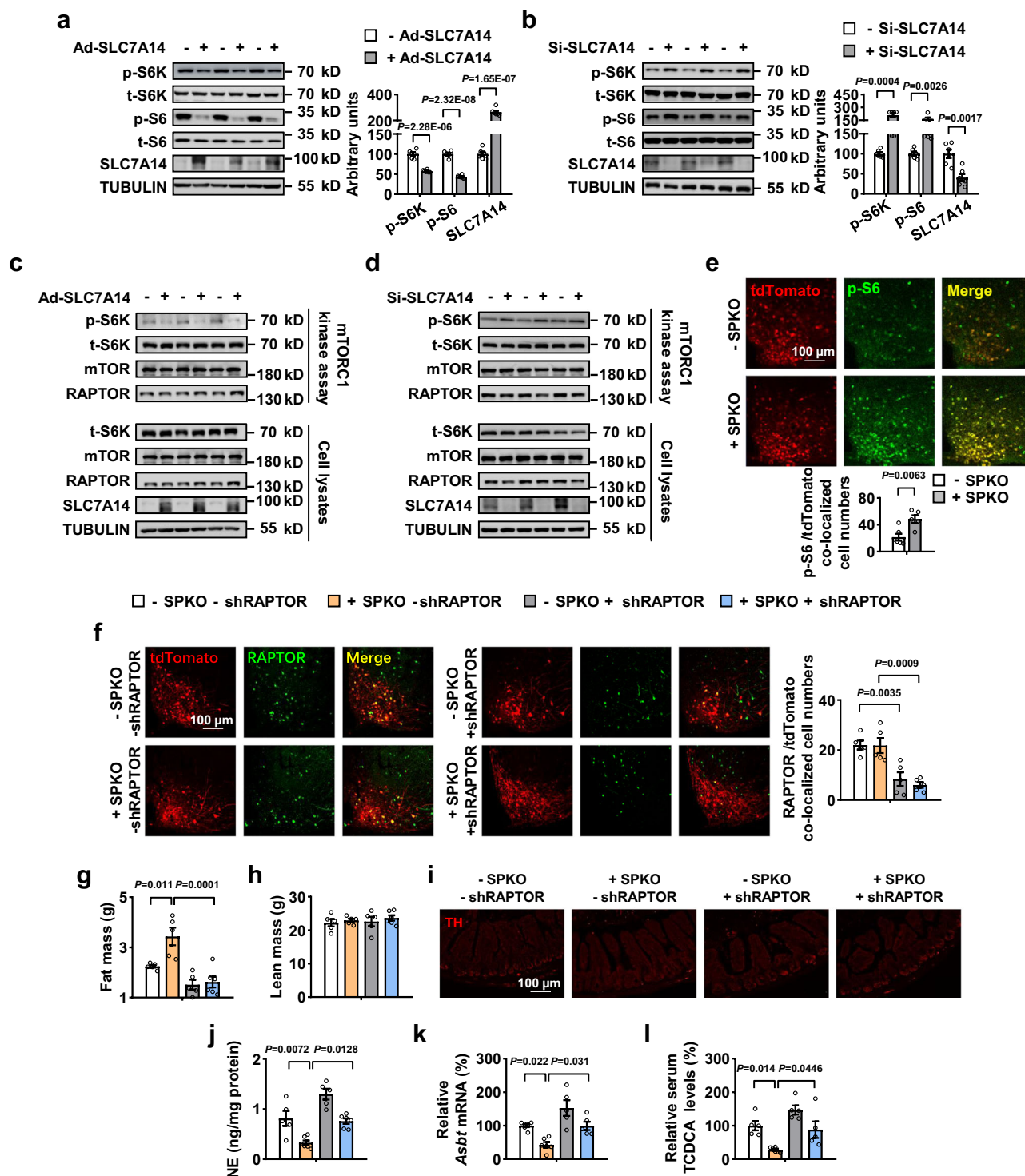


**Fig. 7 | The SLC7A14-induced intestinal sympathetic afferent nerves change is regulated by POMC mTORC1 signaling.** **a, b** P-S6K, t-S6K, p-S6, t-S6, SLC7A14 and TUBULIN proteins in primary hypothalamic cells. **c, d** mTORC1 kinase assays in primary hypothalamic cells. **e** IF staining for tdTomato, p-S6 and merge in ARC sections. **f** IF staining for tdTomato, RAPTOR and merge in ARC sections. **g** Fat mass by NMR. **h** Lean mass by NMR. **i** IF staining for TH. **j** The NE levels of ileum. **k** The mRNA levels of *Asbt* in ileum by RT-PCR. **l** The TCDDA levels of serum. Studies for (**a-d**) were conducted using primary hypothalamic cells, infected with adenovirus expressing green fluorescent protein (- Ad-SLC7A14) or Ad-SLC7A14 (+ Ad-SLC7A14) for 48 h in (**a**) and (**c**), or transfected with double-stranded siRNA targeting mouse SLC7A14 for 72 h in **b** and **d**; **e-l** were conducted using 5 month-old

control mice (- SPK) or mice with SLC7A14 deletion in POMC neurons (+ SPK), and injected with AAVs expressing mCherry (- AAV-RAPTOR) or shRAPTOR (+ AAV-shRAPTOR) in (**f-l**). For **a-b**,  $n=6$ . For **c-d** and **i**,  $n=3$ . For **e**,  $n=6$  (- SPK) and 5 (+SPK). For (**f**)  $n=5$ . For (**g, h**),  $n=5$  (- SPK - shRAPTOR), 5 (+SPK - shRAPTOR), 5 (- SPK + shRAPTOR) and 6 (+SPK + shRAPTOR). For (**j**) and (**l**)  $n=5$  (- SPK - shRAPTOR), 6 (+SPK - shRAPTOR), 5 (- SPK + shRAPTOR) and 6 (+SPK + shRAPTOR). For (**k**),  $n=6$  (- SPK - shRAPTOR), 6 (+SPK - shRAPTOR), 5 (- SPK + shRAPTOR) and 5 (+SPK + shRAPTOR). Data are expressed as the mean  $\pm$  SEM, with individual data points. Data were analyzed by two-tailed unpaired Student's *t*-test (**a, b**, and **e**) or ordinary two-way ANOVA with Tukey's multiple comparisons test (**f-h, j-l**). Source data are provided as a Source Data file.

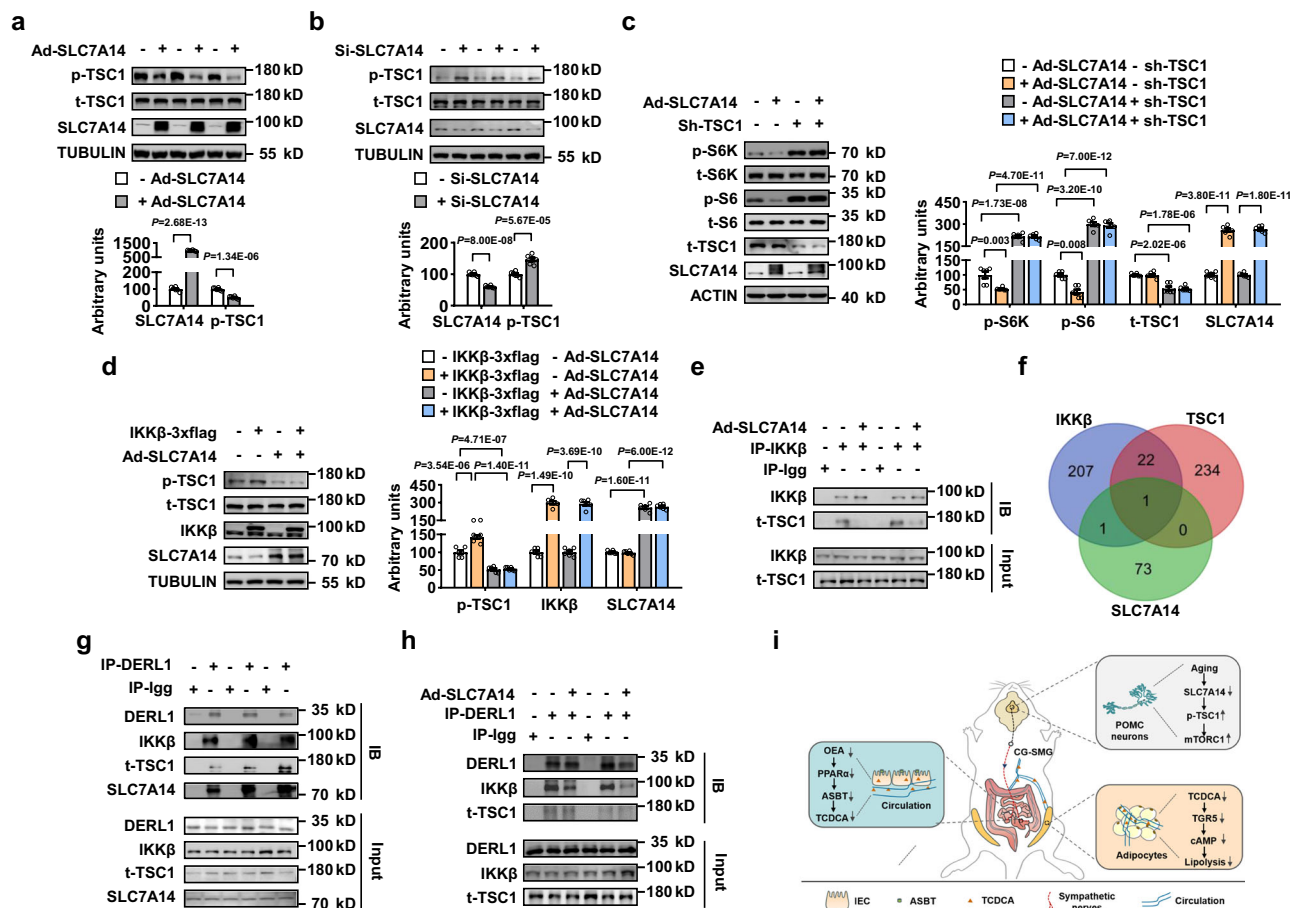


**Fig. 8 | POMC SLC7A14 regulates mTORC1 signaling via TSC1.** **a, b** P-TSC1, t-TSC1, SLC7A14 and TUBULIN proteins in primary hypothalamic cells. **c** p-S6K, t-S6K, p-S6, t-S6, t-TSC1, SLC7A14 and TUBULIN proteins in primary hypothalamic cells. **d** P-TSC1, t-TSC1, IKKβ, SLC7A14 and TUBULIN proteins in primary hypothalamic cells. **e, g, h** Immunoblotting and co-immunoprecipitation in primary hypothalamic cells. **f** Venn chart of interactions for SLC7A14, IKKβ, and TSC1 in HitPredict. **i** Working model. Studies for (**a–e, g**) and **h** were conducted using primary hypothalamic cells, infected with adenovirus expressing green fluorescent protein (- Ad-SLC7A14) or Ad-SLC7A14 (+ Ad-SLC7A14) for 48 h in **a**, or transfected with double-stranded siRNA targeting mouse SLC7A14 for 72 h in **b**, or transfected with double-stranded shRNA targeting mouse TSC1 (+ Sh-TSC1) or without TSC1 shRNA (- Sh-TSC1) for 72 h and infected with adenovirus expressing green fluorescent protein (- Ad-

SLC7A14) or Ad-SLC7A14 (+ Ad-SLC7A14) for 48 h in (**c**), or infected with adenovirus expressing green fluorescent protein (- Ad-SLC7A14) or Ad-SLC7A14 (+ Ad-SLC7A14) and transfected with (+ IKKβ-3xflag) or without (- IKKβ-3xflag) FLAG-tagged IKKβ plasmids for 48 h in **d**; or infected with adenovirus expressing green fluorescent protein (- Ad-SLC7A14) or Ad-SLC7A14 (+ Ad-SLC7A14) for 48 h. Immunoprecipitation (IP) and immunoblotting (IB) were performed using the antibodies indicated in (**e–h**). For (**a–d**) and (**g**),  $n = 6$ . For **e** and **h**,  $n = 3$ . Data are expressed as the mean  $\pm$  SEM, with individual data points. Data were analyzed by two-tailed unpaired Student's *t*-test (**a** and **b**), or ordinary two-way ANOVA with Tukey's multiple comparisons test (**c, d**). Source data are provided as a Source Data file.

PPAR $\alpha$ . The mice recovered for at least 4 weeks before conducting experiments.

### PRV injections

POMC Cre mice, which carrying Ai9 (tdTomato) reporter, were anesthetized and injected with pseudorabies virus (BC-PRV-531-PRV-CAG-EGFP, BrainCase Co., Ltd, China) to intestine. After 6 days, the intestine, CG-SMG and brain were collected.

### Sympathetic denervation

For sympathetic denervation of WAT, both inguinal fat pads of mice were injected with 20  $\mu$ L (1  $\mu$ L per injection) vehicle (saline containing 1% (w/v) ascorbic acid) or 6-hydroxydopamine (6-OHDA, 10  $\mu$ g/ $\mu$ L in saline containing 1% (w/v) ascorbic acid) by microinjector<sup>50</sup>. The mice recovered for 2 weeks before conducting experiments.

For transection of intestinal sympathetic nerves, mice were anesthetized then the abdomen was cut open. Abdominal viscera were gently pulled out and held in warm sterile saline-soaked gauze. The intersection of the descending aorta and the left renal artery was

identified, where the superior mesenteric artery was located. The CG-SMG is wrapped around the superior mesenteric artery and associated lymphatic vessels. Fine forceps and microdissection scissor were used to remove CG-SMG or transect its preganglionic nerve fiber. The mice recovered for at least 2 weeks before conducting experiments.

### Measurements of metabolic parameters

The body fat composition of mice was measured by Bruker Minispec mq10 NMR Analyzer (Bruker, USA). Indirect calorimetry was displayed by comprehensive lab animal monitoring system (Columbus Instruments, USA). Mice were maintained in comprehensive lab animal monitoring system with food and water for 24 h. The dynamic parameters of indirect calorimetry were continuously recorded. The rectal core temperature of mice was measured via the digital thermometer (Physitemp Instruments, USA). The NE and cAMP levels of tissues levels were detected using ELISA kits (Nanjing Jiancheng Bioengineering Institute, China), according to manufacturer's instructions. The cAMP levels of cells were detected by a cAMP kit (TSZ Biosciences, MG1132), according to manufacturer's instructions.

### Histological analysis

Brown adipose tissue (BAT) and white adipose tissue (WAT) were fixed in 4% paraformaldehyde (PFA) overnight, then embedded with paraffin and cut into slices. The slices were stained with hematoxylin and eosin (H&E).

### DNA content

White adipose tissues were resected and weighed for about 50 mg, and genomic DNA was extracted using TRIzol reagent (Cat. No. 15596018, Invitrogen, CA, USA) as described by the manufacturer<sup>51</sup>.

### Glycerol release assays

The white adipose tissues (20–25 mg) of mice were isolated quickly, or adipocytes were cultured and matured, followed by incubation with Krebs-Ringer buffer (12 mM HEPES, 4.9 mM KCl, 121 mM NaCl, 0.33 mM CaCl<sub>2</sub> and 1.2 mM MgSO<sub>4</sub>) containing 3.0% fatty acid-free BSA and 3 mM glucose, with 10 μM FSK at 37 °C<sup>52</sup>. The supernatants were collected after incubation for 0.5 h, 1 h, or 2 h. For primary adipocytes, cells were incubated with Krebs-Ringer buffer, with or without 10 μM FSK at 37 °C for 2 h. The supernatants were collected after incubation for 1 h or 2 h. The glycerol levels of samples were analyzed by glycerol assay kit (Nanjing Jiancheng Bioengineering Institute, China).

### Primary hypothalamic cells isolation and treatments

Mouse primary hypothalamic cells were prepared from WT mice born within 24 h by trypsin dispersion<sup>53</sup>. Cells were incubated in neurobasal medium (Cat. No. C11995500CP, ThermoFisher) with B27 supplement (Cat. No. A3582801, ThermoFisher), 100 μg/mL streptomycin sulfate and 100 units/mL penicillin (Cat. No.60162E576, YEASEN)<sup>51</sup>. All cells were maintained at 37 °C and 5% CO<sub>2</sub>. Cells were transfected with double-stranded siRNA targeting mouse SLC7A14 (Cat. No. sc-153580, Santa Cruz) or shRNA TSC1 (Hanbio Tech, China) by using Lipofectamine 3000 (Cat. No. L3000015, Invitrogen). The target shRNA sequence of TSC1 was 5'- TTGTCACATCCGTATAGTAAA-3'. Cells were infected with adenovirus expressing SLC7A14 (+Ad-SLC7A14) or expressing GFP adenovirus (- Ad-SLC7A14) at a dose of 10<sup>7</sup> pfu/well in 12-well plates.

### Primary adipocytes isolation and differentiation

For primary adipocytes isolation, the adipose tissues were prepared from mice, cut into pieces, and digested with collagenase I at 37 °C. After 1 h, cells were collected by centrifugation at 600 × g for 5 min, resuspended with PBS containing streptomycin sulfate and penicillin and filtrated with 70 μm cell strainer. Cells were incubated in low-glucose DMEM (Cat.No.10-014-CVR, Corning) with 10% fetal bovine serum (Cat. No.04-001-1A, Biological Industries), and maintained at 37 °C and 5% CO<sub>2</sub>.

For white adipocyte differentiation, cells were cultured in high-glucose DMEM (Cat.No.C11995500CP, ThermoFisher) containing 10% FBS, 50 μM indomethacin, 0.5 mM isobutyl methylxanthine, 10 μg/mL insulin and 1 μM dexamethasone for 3 days. Then replaced with high-glucose DMEM containing 10 μg/mL insulin and 10% FBS until harvest<sup>54</sup>. Cells were treated with TCDCA or SQ22536 (HY-100396, MCE) or INT777 (HY-15677, MCE), or transfected with double-stranded siRNA targeting mouse TGR5. The target siRNA sequence of TGR5 was 5'-CUGGAACUCUGUUAUCGCUTT-3'.

### Immunoblotting and co-immunoprecipitation

Immunoblotting and co-immunoprecipitation assays<sup>55</sup> were performed in primary hypothalamic cells with the following primary antibodies: anti- DERL1 (1:1000, Cat. No. A8508, ABclonal); anti- IKBKB (1:1000, Cat. No. 15649-1-AP, Proteintech).

### mTORC1 kinase assays

The mTORC1 kinase assays<sup>28</sup> were performed in Primary hypothalamic cells. Primary hypothalamic cells were harvested and lysed. The

protein content of each sample was 1 mg/mL. Addition of anti-mTOR antibody (1:100, Cat. No. 66888-1-Ig, Proteintech) into each sample and incubated with gentle rotation for 2 h. Then protein G-sepharose was added and incubated for 2 h. Immunoprecipitates were washed 4 times, followed by adding 45 μL kinase buffer (25 mM HEPES pH 7.5, 100 mM potassium acetate, 1 mM MgCl<sub>2</sub>) containing 500 μM ATP (Cat. No. A600020-0005, sangon, Shanghai, China) and 500 ng inactive S6K (Cat. No. P02664, Solarbio) to each sample and incubated at 37 °C for 30 min, terminated by the addition of 2 × SDS sample buffer and analyzed by immunoblotting.

### Untargeted metabolomics analysis

The metabolite assessment of samples was performed by untargeted metabolomics at Novogene Biotech Co., Ltd. Serum was collected from control or overexpression of SLC7A14 in POMC neuron mice. The serum samples (100 μL) were resuspended with prechilled 80% methanol and 0.1% formic acid by well vortex. Then the samples were incubated on ice for 5 min and centrifuged at 15,000 g, 4 °C for 20 min. Some of supernatant was diluted to final concentration containing 53% methanol by LC-MS grade water. The samples were subsequently transferred to a fresh Eppendorf tube and then centrifuged at 15000 g, 4 °C for 20 min. The QC sample was prepared by mixing an equal aliquot of the supernatant from all of samples. All samples were injected in the LC-MS/MS system in a randomized order. UHPLC-MS/MS analyses were performed using a Vanquish UHPLC system (ThermoFisher, Germany) coupled with an Orbitrap Q ExactiveTMHF-X mass spectrometer (Thermo Fisher, Germany). Samples were injected onto a Hypesil Gold column (100 × 2.1 mm, 1.9 μm). The mobile phase consisted of eluent A (5 mM ammonium acetate in water, pH 9.0) and eluent B (Methanol). The solvent gradient was set as the following: 2% B, 1.5 min; 2–100% B, 12.0 min; 100% B, 14.0 min; 100–2% B, 14.1 min; 2% B, 17 min. B. The column flow rate was 0.2 mL/min, and the injection volume was 1 μL. The raw data files generated by UHPLC-MS/MS were processed using the Compound Discoverer 3.1 (CD3.1, ThermoFisher) to perform peak alignment, peak picking, and quantitation for each metabolite. There was 5 ppm tolerance used for the matching against a database. The normalized data was used to predict the molecular formula based on mass number deviation (ppm), additive ions, molecular ion peaks and fragment ions. And then peaks were matched with the mzCloud (<https://www.mzcloud.org/>), mzVault and MassList database to obtain the accurate qualitative and relative quantitative results. Statistical analyses were performed using the statistical software R (R version R-3.4.3), Python (Python 2.7.6 version) and CentOS (CentOS release 6.6). The data normalization was based on QC (Quality Control) samples. The Pearson correlation coefficient between QC samples was used to assess the stability of metabolomics data sets. Principal components analysis (PCA) was performed at metaX. We applied univariate analysis (*t*-test) to calculate the statistical significance (*P*-value). The metabolites with VIP > 1 and *P*-value < 0.05 and fold change ≥ 2 or FC ≤ 0.5 were considered to be differential metabolites. The metabolites were annotated using the KEGG database, HMDB database and LIPID MAPS database. We used a list of a differential annotated metabolites (Supplementary Data 1) to perform metabolite set enrichment analysis (MSEA) on MetaboAnalyst 5.0. We used Enrichment Analysis module in MetaboAnalyst 5.0, and selected chemical structures (main-class) metabolite set library for MSEA. The raw LC-MS data has been uploaded on MetaboLights (MTBLS9872) and shown in Supplementary Data 1.

### Bile acids measurements

The bile acids extraction of tissues, feces or serum was performed as previously described<sup>56</sup>, and quantified by LC-MS/MS (Shanghai Institute for Biological Sciences, Chinese Academy of Sciences). The samples (60 μL) were resuspended with 1 mL prechilled acetonitrile by well vortex, and incubated at 4 °C for 2 h, then centrifuged at 11,000 g, 4 °C for 20 min. Freeze drying and vacuum evaporation of the supernatant.

Then the samples were redissolved in 50% methanol and 5  $\mu$ L of sample was injected into the LC-MS/MS system analysis. LC-MS/MS analyses were performed using an Agilent 1200 high performance LC system (Agilent Technologies, USA) coupled with a 4000Q TRAP triple quadrupole (QQQ) mass spectrometer (AB Sciex, USA). Turbo Ion Spray source was operated in the negative-ion multiple-reaction monitoring (MRM) mode. The MRM transitions of 5 bile acids were shown in Table S1. The ESI-MS parameters were the ion spray voltage,  $-4500$  V; nebulizer gas (N<sub>2</sub>), 50 units; curtain gas (N<sub>2</sub>), 15 units; collision gas (N<sub>2</sub>), medium. The drying gas (N<sub>2</sub>) flow and temperature were 50 units and  $500$  °C, respectively. For LC-MS/MS quantification of differential bile acids, samples were injected onto a Thermo scientific Acclaim C30 column ( $2.1 \times 250$  mm,  $3 \mu$ m). The column flow rate was  $0.2$  mL/min, the column temperature was  $45$  °C, and the autosampler was kept at  $4$  °C. The eluents were eluent A ( $0.01\%$  formic acid in water) and eluent B (acetonitrile with  $0.01\%$  formic acid). The binary elution gradient was  $25\%$  B to  $40\%$  B in 12 min and then  $40\%$  to  $75\%$  B in 14 min. The column was washed with  $100\%$  B for 3 min and equilibrated with  $25\%$  B for 7 min between injections.

### Immunofluorescence (IF) staining assays

The brain slices were prepared as previously described<sup>49</sup>. The IF staining of SLC7A14 was performed with a TSA fluorescence system kit (APEX BIO) according to the manufacturer's protocol. The IF staining of p-S6 and RAPTOR were performed according to the manufacturer's protocol. Primary antibodies used in IF experiments: anti-SLC7A14 (1:300, Cat. No. BMP042, MBL International); anti-p-S6 (ser235/235) (1:300, Cat. No. 4857S, Cell Signaling Technology); anti-RAPTOR (1:300, Cat. No. 21097-1-AP, Proteintech); anti-Hamartin/TSC1 (1:500, Cat. No. A0720, ABclonal); anti-Phospho-Hamartin/TSC1 (Ser511) (1:500, Cat. No. 80340-1-RR, Proteintech).

### RNA isolation and relative quantitative RT-PCR

TRIzol reagent (Cat. No. 15596018, Invitrogen, CA, USA) was used for extracting RNA. High-Capacity cDNA Reverse Transcription Kit (Cat. No. RR037A, TaKaRa) was used for mRNA reverse transcription. SYBR Green I Master Mix reagent by ABI 7900 system (Applied Biosystems, USA) was used for quantitative real-time PCR. The sequences of primers used are listed in Table S2.

### Western Blot analysis

Western blot analysis was performed as previously described (Jiang et al.<sup>28</sup>). Proteins were visualized by ECL (Cat. No. P0018FM, Beyotime). Band intensities were measured using e-BLOT Touch Imager (Shanghai Yibote Optoelectronic Technology Co., Ltd, China). Primary antibodies used were as follows: anti-Phospho-HSL (Ser660) (1:1000, Cat. No. 45804, Cell Signaling Technology); anti-HSL (1:1000, Cat. No. 4107, Cell Signaling Technology); anti-Phospho-PKA Substrate (1:1000, Cat. No. 9621, Cell Signaling Technology); anti-Phospho-p70 S6 Kinase (Thr389) (1:1000, Cat. No. 9234, Cell Signaling Technology); anti-p70 S6 Kinase (1:1000, Cat. No. 2708, Cell Signaling Technology); anti-p-S6 (ser235/235) (1:1000, Cat. No. 4857S, Cell Signaling Technology); anti-t-S6 (1:1000, Cat. No. 2217 s, Cell Signaling Technology); anti-UCP1 (1:10000, Cat. No. ab209483, Abcam); anti-SLC7A14 (1:500, Cat. No. HPA045929-100UL, Sigma); anti-Phospho-Hamartin/TSC1 (Ser511) (1:1000, Cat. No. 80340-1-RR, Proteintech); (Cat. No. 15184-1-AP, Proteintech); anti-RAPTOR (1:1000, Cat. No. 21097-1-AP, Proteintech); anti-IKBKB (1:1000, Cat. No. 15649-1-AP, Proteintech); anti-mTOR (1:1000, Cat. No. 66888-1-Ig, Proteintech); anti-TUBULIN (1:2500, Cat. No. 66031-1-Ig, Proteintech); anti-ACTIN (1:2500, Cat. No. 66009-1-Ig, Proteintech); anti-ASBT (1:1000, Cat. No. 25245-1-AP, Proteintech); anti-Fatty Acid Synthase (1:1000, Cat. No. 610963, BD Biosciences); anti-CD36 (1:1000, Cat. No. A5792, ABclonal); anti-DERL1 (1:1000, Cat. No. A8508, ABclonal); anti-Tyrosine Hydroxylase (1:1000, Cat. No. AB152, Millipore); anti-Hamartin/TSC1 (1:500, Cat. No. A0720,

ABclonal); anti-Phospho-Hamartin/TSC1 (Ser511) (1:500, Cat. No. 80340-1-RR, Proteintech).

### Quantification and statistical analysis

Statistical analyses were performed in GraphPad Prism, version 8.0 (GraphPad Software, CA, USA). All values were represented as the mean  $\pm$  the standard error of the mean (SEM). Individual data points on each histogram were also shown with individual variability of their measures represented and also shown in figure legends. For two groups comparisons, two-tailed unpaired Student's *t*-test was used. For multiple group comparisons, ordinary one-way ANOVA, two-way ANOVA or two-way RM ANOVA with Geisser-Greenhouse's correction was used, followed by Dunnett's or Tukey's multiple comparisons test. MetaboAnalyst 5.0 was used for metabolite set enrichment analysis (MSEA). Results were considered statistically significant at *P*-value  $< 0.05$ . \**p*  $< 0.05$ , \*\**p*  $< 0.01$ , \*\*\**p*  $< 0.001$ , \*\*\*\**p*  $< 0.0001$ .

### Reporting summary

Further information on research design is available in the Nature Portfolio Reporting Summary linked to this article.

### Data availability

The authors declare that all data supporting the findings of this study are available within this paper and its Supplementary Files. The metabolomics data generated in this study have been deposited in the MetaboLights database under accession code [MTBLS9872](https://www.ebi.ac.uk/metabolights/MTBLS9872) and also include in Supplementary Data 1. The single cell analysis use [GSE188646](https://www.ebi.ac.uk/metabolights/GSE188646). Source data are provided with this paper.

### References

- Kuk, J. L., Saunders, T. J., Davidson, L. E. & Ross, R. Age-related changes in total and regional fat distribution. *Ageing Res. Rev.* **8**, 339–348 (2009).
- Santos, A. L. & Sinha, S. Obesity and aging: molecular mechanisms and therapeutic approaches. *Ageing Res. Rev.* **67**, 101268 (2021).
- Kim, J. G. & Horvath, T. L. mTOR signaling fades POMC neurons during aging. *Neuron* **75**, 356–357 (2012).
- Camell, C. D. et al. Inflammasome-driven catecholamine catabolism in macrophages blunts lipolysis during ageing. *Nature* **550**, 119–123 (2017).
- Gao, H. et al. Age-induced reduction in human lipolysis: a potential role for adipocyte noradrenaline degradation. *Cell Metab.* **32**, 1–3 (2020).
- Li, Q. O. Y., Soro-Arnaiz, I. & Aragonés, J. Age-dependent obesity and mitochondrial dysfunction. *Adipocyte* **6**, 161–166 (2017).
- Pidoux, G. et al. Optic atrophy 1 is an A-kinase anchoring protein on lipid droplets that mediates adrenergic control of lipolysis. *EMBO J.* **30**, 4371–4386 (2011).
- Camell, C. D. et al. Aging induces an Nlrp3 inflammasome-dependent expansion of adipose B cells that impairs metabolic homeostasis. *Cell Metab.* **30**, 1024–1039.e1026 (2019).
- Yang, S. B. et al. Rapamycin ameliorates age-dependent obesity associated with increased mTOR signaling in hypothalamic POMC neurons. *Neuron* **75**, 425–436 (2012).
- Kinyua, A. W., Yang, D. J., Chang, I. & Kim, K. W. Steroidogenic factor 1 in the ventromedial nucleus of the hypothalamus regulates age-dependent obesity. *PLoS ONE* **11**, e0162352 (2016).
- Jais, A. & Brüning, J. C. Arcuate nucleus-dependent regulation of metabolism-pathways to obesity and diabetes mellitus. *Endocr. Rev.* **43**, 314–328 (2022).
- Gómez-Valadés, A. G. et al. Mitochondrial cristae-remodeling protein OPA1 in POMC neurons couples Ca<sup>2+</sup> homeostasis with adipose tissue lipolysis. *Cell Metab.* **33**, 1820–1835.e1829 (2021).
- Scherer, T. et al. Brain insulin controls adipose tissue lipolysis and lipogenesis. *Cell Metab.* **13**, 183–194 (2011).

14. Zeng, W. et al. Sympathetic neuro-adipose connections mediate leptin-driven lipolysis. *Cell* **163**, 84–94 (2015).
15. Chouchani, E. T. & Kajimura, S. Metabolic adaptation and maladaptation in adipose tissue. *Nat. Metab.* **1**, 189–200 (2019).
16. Frühbeck, G., Méndez-Giménez, L., Fernández-Formoso, J. A., Fernández, S. & Rodríguez, A. Regulation of adipocyte lipolysis. *Nutrition Res. Rev.* **27**, 63–93 (2014).
17. Lawson, E. A. The effects of oxytocin on eating behaviour and metabolism in humans. *Nat. Rev. Endocrinol.* **13**, 700–709 (2017).
18. Donato, J., Jr., Wasinski, F., Furigo, I. C., Metzger, M. & Frazão, R. Central regulation of metabolism by growth hormone. *Cells* **10**, 129 (2021).
19. Beckermann, K. E. et al. CD28 costimulation drives tumor-infiltrating T cell glycolysis to promote inflammation. *JCI Insight* **5**, e138729 (2020).
20. Burford, N. G., Webster, N. A. & Cruz-Topete, D. Hypothalamic-pituitary-adrenal axis modulation of glucocorticoids in the cardiovascular system. *Int. J. Mol. Sci.* **18**, 2150 (2017).
21. Perino, A., Demagny, H., Velazquez-Villegas, L. & Schoonjans, K. Molecular physiology of bile acid signaling in health, disease, and aging. *Physiol. Rev.* **101**, 683–731 (2021).
22. Zhang, G. et al. Hypothalamic programming of systemic ageing involving IKK- $\beta$ , NF- $\kappa$ B and GnRH. *Nature* **497**, 211–216 (2013).
23. Chang, H. C. & Guarente, L. SIRT1 mediates central circadian control in the SCN by a mechanism that decays with aging. *Cell* **153**, 1448–1460 (2013).
24. Kim, J. & Guan, K. L. mTOR as a central hub of nutrient signalling and cell growth. *Nat. Cell Biol.* **21**, 63–71 (2019).
25. Kocalis, H. E. et al. Rictor/mTORC2 facilitates central regulation of energy and glucose homeostasis. *Mol. Metab.* **3**, 394–407 (2014).
26. Lee, D. F. et al. IKK beta suppression of TSC1 links inflammation and tumor angiogenesis via the mTOR pathway. *Cell* **130**, 440–455 (2007).
27. Jaenecke, I. et al. A chimera carrying the functional domain of the orphan protein SLC7A14 in the backbone of SLC7A2 mediates trans-stimulated arginine transport. *J. Biol. Chem.* **287**, 30853–30860 (2012).
28. Jiang, X. et al. SLC7A14 imports GABA to lysosomes and impairs hepatic insulin sensitivity via inhibiting mTORC2. *Cell Rep.* **42**, 111984 (2023).
29. Jin, Z. B. et al. SLC7A14 linked to autosomal recessive retinitis pigmentosa. *Nat. Commun.* **5**, 3517 (2014).
30. Giffen, K. P. et al. Mutation of SLC7A14 causes auditory neuropathy and retinitis pigmentosa mediated by lysosomal dysfunction. *Sci. Adv.* **8**, eabk0942 (2022).
31. Zoncu, R. et al. mTORC1 senses lysosomal amino acids through an inside-out mechanism that requires the vacuolar H<sup>(+)</sup>-ATPase. *Science* **334**, 678–683 (2011).
32. Haemmerle, G. et al. Defective lipolysis and altered energy metabolism in mice lacking adipose triglyceride lipase. *Science* **312**, 734–737 (2006).
33. Carper, D. et al. Atrial natriuretic peptide orchestrates a coordinated physiological response to fuel non-shivering thermogenesis. *Cell Rep.* **32**, 108075 (2020).
34. Qi, Y. C. et al. Taurochenodeoxycholic acid mediates cAMP-PKA-CREB signaling pathway. *Chin. J. Nat. Med.* **18**, 898–906 (2020).
35. Grabner, G. F., Xie, H., Schweiger, M. & Zechner, R. Lipolysis: cellular mechanisms for lipid mobilization from fat stores. *Nat. Metab.* **3**, 1445–1465 (2021).
36. Kim, S. H. et al. Antagonism of VEGF-A-induced increase in vascular permeability by an integrin  $\alpha$ 3 $\beta$ 1-Shp-1-cAMP/PKA pathway. *Blood* **120**, 4892–4902 (2012).
37. Thomas, C. et al. TGR5-mediated bile acid sensing controls glucose homeostasis. *Cell Metab.* **10**, 167–177 (2009).
38. Yang, N. et al. ASBT(SLC10A2): A promising target for treatment of diseases and drug discovery. *Biomed. Pharmacother.* **132**, 110835 (2020).
39. Jung, D., Fried, M. & Kullak-Ublick, G. A. Human apical sodium-dependent bile salt transporter gene (SLC10A2) is regulated by the peroxisome proliferator-activated receptor alpha. *J. Biol. Chem.* **277**, 30559–30566 (2002).
40. Bowen, K. J. et al. Oleic acid-derived oleoylethanolamide: a nutritional science perspective. *Prog. Lipid Res.* **67**, 1–15 (2017).
41. Xiao, F. et al. Reduced hepatic bradykinin degradation accounts for cold-induced BAT thermogenesis and WAT browning in male mice. *Nat. Commun.* **14**, 2523 (2023).
42. Henske, E. P., Jóźwiak, S., Kingswood, J. C., Sampson, J. R. & Thiele, E. A. Tuberous sclerosis complex. *Nat. Rev. Dis. Primers* **2**, 16035 (2016).
43. Patil, A., Nakai, K. & Nakamura, H. HitPredict: a database of quality assessed protein-protein interactions in nine species. *Nucleic Acids Res.* **39**, D744–749, (2011).
44. Li, L. et al. Derlin1 functions as an oncogene in cervical cancer via AKT/mTOR signaling pathway. *Biol. Res.* **52**, 8 (2019).
45. Puente-Ruiz, S. C. & Jais, A. Reciprocal signaling between adipose tissue depots and the central nervous system. *Front Cell Dev. Biol.* **10**, 979251 (2022).
46. Biglari, N. et al. Functionally distinct POMC-expressing neuron subpopulations in hypothalamus revealed by intersectional targeting. *Nat. Neurosci.* **24**, 913–929 (2021).
47. Pan, S. et al. Stimulation of hypothalamic oxytocin neurons suppresses colorectal cancer progression in mice. *eLife* **10**, e67535 (2021).
48. Piomelli, D. A fatty gut feeling. *Trend Endocrinol. Metab. TEM* **24**, 332–341 (2013).
49. Yuan, F. et al. Activation of GCN2/ATF4 signals in amygdalar PKC- $\delta$  neurons promotes WAT browning under leucine deprivation. *Nat. Commun.* **11**, 2847 (2020).
50. Dodd, G. T. et al. Leptin and insulin act on POMC neurons to promote the browning of white fat. *Cell* **160**, 88–104 (2015).
51. Deng, Y. et al. SGK1/FOXO3 signaling in hypothalamic POMC neurons mediates glucocorticoid-increased adiposity. *Diabetes* **67**, 569–580 (2018).
52. Liew, C. W. et al. Ablation of TRIP-Br2, a regulator of fat lipolysis, thermogenesis and oxidative metabolism, prevents diet-induced obesity and insulin resistance. *Nat. Med.* **19**, 217–226 (2013).
53. Liu, Y., Kamitakahara, A., Kim, A. J. & Aguilera, G. Cyclic adenosine 3',5'-monophosphate responsive element binding protein phosphorylation is required but not sufficient for activation of corticotropin-releasing hormone transcription. *Endocrinology* **149**, 3512–3520 (2008).
54. Liu, K. et al. Scd1 controls de novo beige fat biogenesis through succinate-dependent regulation of mitochondrial complex II. *Proc. Natl Acad. Sci. USA* **117**, 2462–2472 (2020).
55. Deng, J. et al. Autophagy inhibition prevents glucocorticoid-increased adiposity via suppressing BAT whitening. *Autophagy* **16**, 451–465 (2020).
56. Song, X. et al. Microbial bile acid metabolites modulate gut ROR $\gamma$ (+) regulatory T cell homeostasis. *Nature* **577**, 410–415 (2020).

## Acknowledgements

This work was supported by grants from the National Key R&D Program of China (2018YFA0800600 to F.G.), the National Natural Science Foundation (92357304, 31830044 and 91957207 to F.G.; 82270905 to F.X.; 82370811 to F.Y.; 82300939 to X.J.), Shanghai leading talent program (to F.G.), and Postdoctoral Fellowship Program of CPSF (GZC20230479 to X.J. and GZC20230478 to H.J.), China Postdoctoral Science Foundation (2023M740695 to X.J.).



## Author contributions

X.J. and K.L. designed and carried out overall experiments, analyzed data, wrote, reviewed and edited the manuscript. P.L., F.X., H.J., S.W., M.T., F.Y., S.C. and S.N. assisted with mouse experiments and cultured cell studies. Z.L. developed the LC-MS/MS platform to measure the Bile acids levels. X.L. Y.S. and B.P. provided research materials and contributed to discussion. F.G. directed the research, contributed to discussion, wrote, reviewed and edited the manuscript.

## Competing interests

The authors declare no competing interests.

## Additional information

**Supplementary information** The online version contains supplementary material available at <https://doi.org/10.1038/s41467-024-52059-1>.

**Correspondence** and requests for materials should be addressed to Feifan Guo.

**Peer review information** *Nature Communications* thanks Xiangping Lin and the other anonymous reviewers for their contribution to the peer review of this work. A peer review file is available.

**Reprints and permissions information** is available at <http://www.nature.com/reprints>

**Publisher's note** Springer Nature remains neutral with regard to jurisdictional claims in published maps and institutional affiliations.

**Open Access** This article is licensed under a Creative Commons Attribution-NonCommercial-NoDerivatives 4.0 International License, which permits any non-commercial use, sharing, distribution and reproduction in any medium or format, as long as you give appropriate credit to the original author(s) and the source, provide a link to the Creative Commons licence, and indicate if you modified the licensed material. You do not have permission under this licence to share adapted material derived from this article or parts of it. The images or other third party material in this article are included in the article's Creative Commons licence, unless indicated otherwise in a credit line to the material. If material is not included in the article's Creative Commons licence and your intended use is not permitted by statutory regulation or exceeds the permitted use, you will need to obtain permission directly from the copyright holder. To view a copy of this licence, visit <http://creativecommons.org/licenses/by-nc-nd/4.0/>.

© The Author(s) 2024